HAL open science

Paleoenvironmental evolution of Picos de Europa (Spain) during marine isotopic stages 5c to 3 combining glacial reconstruction, cave sedimentology and paleontological findings

Daniel Ballesteros, Adrián Álvarez-Vena, Mael Monod-del Dago, Laura Rodríguez-Rodríguez, Jorge Sanjurjo-Sánchez, Diego Álvarez-Lao, Carlos Pérez-Mejías, Pablo Valenzuela, Irene Defelipe, César Laplana, et al.

To cite this version:

Daniel Ballesteros, Adrián Álvarez-Vena, Mael Monod-del Dago, Laura Rodríguez-Rodríguez, Jorge Sanjurjo-Sánchez, et al.. Paleoenvironmental evolution of Picos de Europa (Spain) during marine isotopic stages 5c to 3 combining glacial reconstruction, cave sedimentology and paleontological findings. Quaternary Science Reviews, 2020, 248, pp.106581 -. 10.1016/j.quascirev.2020.106581 . hal-03493365

HAL Id: hal-03493365

https://hal.science/hal-03493365v1

Submitted on 17 Oct 2022

HAL is a multi-disciplinary open access archive for the deposit and dissemination of scientific research documents, whether they are published or not. The documents may come from teaching and research institutions in France or abroad, or from public or private research centers.

L'archive ouverte pluridisciplinaire **HAL**, est destinée au dépôt et à la diffusion de documents scientifiques de niveau recherche, publiés ou non, émanant des établissements d'enseignement et de recherche français ou étrangers, des laboratoires publics ou privés.

Distributed under a Creative Commons Attribution - NonCommercial 4.0 International License

Version of Record: https://www.sciencedirect.com/science/article/pii/S0277379120305436
Manuscript_a8935592a056fac642d5fa0002f2a47a

Paleoenvironmental evolution of Picos de Europa (Spain) during Marine Isotopic Stages 5c to 3 combining glacial reconstruction, cave sedimentology and paleontological findings.

Daniel Ballesteros (1), Adrián Álvarez-Vena (2), Mael Monod-Del Dago (3), Laura Rodríguez-Rodríguez (4, 5), Jorge Sanjurjo-Sánchez (6), Diego Álvarez-Lao (2), Carlos Pérez-Mejías (7), Pablo Valenzuela (8), Irene DeFelipe (9), César Laplana (10), Hai Cheng (7), Montserrat Jiménez-Sánchez (2).

(1) UMR 6266 - IDEES, University of Rouen-Normandie/CNRS. Mont Saint-Aignan CEDEX, France. daniel.ballesteros@univ-rouen.fr

(2) Department of Geology, University of Oviedo. c/ Jesús Arias de Velasco s/n, 33005, Oviedo. adrian@picos-europa.com, dalao@geol.uniovi.es, mjimenez@geol.uniovi.es

(3) Université Paris 1 Panthéon-Sorbonne, 191 rue Saint Jacques, 75005 Paris. maelmdd@gmail.com

(4) Laboratoire de Géographie Physique (UMR 8591, CNRS). 1 Place Aristide Briand, 92195 Meudon CEDEX, France. lelydriguez@gmail.com

(5) Departamento de Ciencias de la Tierra y Física de la Materia Condensada, Universidad de Cantabria. Avenida de los Castros 48, 39005 Santander, Spain

(6) University Institute of Geology Isidro Parga Pondal, University of A Coruña. Campus de Elviña s/n, 15011, A Coruña, Spain. jsanjurjo@udc.es

(7) Institute of Global Environmental Change, Xi'an Jiaotong University, Xi'an, 710049, China. perezmegias@mail.xjtu.edu.cn, cheng021@xjtu.edu.cn.

(8) TRAGSATEC S.A. c/ Julián Camarillo 6B, 28037, Madrid, Spain. pablo.valenzuela.mendizabal@gmail.com

(9) Geosciences Barcelona (CSIC). c/ Lluís Solé i Sabaris s/n 08028 Barcelona. irene.defelipe@gmail.com

(10) Museo Arqueológico Regional de la Comunidad de Madrid. Pza. Bernardas s/n, 28801, Alcalá de Henares, Spain. cesar.laplana@gmail.com

ABSTRACT

In glaciated areas, the environmental evolution before MIS 2 is usually poorly constrained mainly due to the later glacial erosion during the global Last Glacial Maximum (LGM). However, in carbonate areas, karst caves can preserve records of pre-LGM paleoenvironment interest. We studied a cave

© 2020 published by Elsevier. This manuscript is made available under the CC BY NC user license
https://creativecommons.org/licenses/by-nc/4.0/

(1350 m altitude) to establish the paleoenvironmental evolution of a glaciated karst area in Picos de Europa (SW Europe). For this objective, a glacial reconstruction, cave sedimentology analyses, macro- and micromammal remains are combined with ten U-Th, OSL and AMS ^{14}C ages. The paleo-glacial reconstruction indicates glaciers descended down to 810–1040 m of altitude covering an area in 36.18 km^2 of the surroundings of Covadonga Lakes during the glacial local maximum, with the equilibrium line altitude located at 1524 ± 36 m. The geomorphological study of the cave and the U-Th and OSL dates reveal the presence of three allochthonous alluvial sediment sequences at 132-135, 98-60 and ca. 36 ka. These last two sequences would come from the erosion of fluvioglacial sediments including teeth fragments of *Pliomys coronensis* (=*P. lenki*), an unusual species in NW Spain in high areas during the Upper Pleistocene. In addition, found remains of chamois (*Rupicapra pyrenaica*) dated in 37–33 cal ka BP constitutes the oldest evidence of chamois above 800 m asl in the region. All the presented data indicate the development of alpine glacier-free areas covered by fluvioglacial sediments at ca. 1450 m altitude at 98-60 and 37–33 ka, corresponding to glacial retreat stages.

KEYWORDS

Karst, glacial reconstruction, paleoenvironment, *Pliomys coronensis*, *Rupicapra pyrenaica*.

1. INTRODUCTION

Paleoenvironmental records corresponding to Marine Isotope Stages (MIS) 4–3 are relatively scarce in glaciated mountains, mainly due to glacier erosion associated to the Last Glacial Maximum (LGM) of MIS 2. In areas made of limestone or another soluble rock, karst caves often preserve abundant additional paleoenvironmental evidence sheltered from surface weathering (Häuselmann, 2013). Cave evidence can be compared with surface landforms and sedimentary logs in order to reconstruct the past environmental evolution of a territory, improving our understanding on glacial advances and retreats (Mylroie and Mylroie, 2004; Bočić et al., 2012; Weremeichik and Mylroie 2014).

In glaciated areas, endokarst sedimentary records are mainly represented by speleothems and fluvial deposits, commonly originated during the Pliocene–Upper Pleistocene (Audra et al., 2006). Among the speleothems, stalagmites frequently grow during interglacial periods, when high CO_2 concentrations related to warm environments favors carbonate dissolution and precipitation in the karst conduits

(Isola et al., 2019; Tîrlă et al., in press). However, its growth is not only limited to interglacials, as can be seen in a compilation of stalagmite records from Western Europe (Lechleitner et al., 2018). During glaciations, glacial melting often affects karst aquifers favoring coarse grain sedimentation or erosion processes according to glacial evolution. Pioneering works by Ford (1971, 1979) and Glover (1977) already established that main endokarst detrital aggradation episodes are coeval with glacial retreats and, occasionally, with the onset of glacial advances. Glaciers can inject sediments in cave passages located at more than 1 km depth in glaciated areas (Audra et al., 2002), as well as in shallow caves influenced by glacial outwash and located at distances of over 1000 km from the icefield (Mylroie, 1984). Since these sediments result from the glacial erosion of limestone, they are mostly formed of carbonate-rich silt, the so-called “glacial rock-flour” or “glacial milk” (Bočić et al., 2012; Weremeichik and Mylroie, 2014). In addition, cave detrital aggradation may also include allochthonous cobbles and gravels derived from the erosion of any lithology outcropping in the catchment area (Audra et al., 2002; Ballesteros et al., 2017). In temperate settings, glacial valley incision dominantly occurs during glaciations (Häuselmann et al., 2007). Therefore, the increase of hydraulic gradients in the endokarst favours the development of torrential water flow that broadly erodes and evacuates cave sediments, simultaneously to the general enlargement of previous vadose canyons (Plan et al., 2009; Adamson et al., 2014). However, if glaciers reach the bottom of fluvial valleys, karst springs can be blocked by till, thus triggering inundations in the endokarst (Skoglund et al., 2010). During these floods, glacial carbonate silt decants forming rhythmic slackwater deposits related to sedimentary changes in underground lakes (Weremeichik and Mylroie, 2014; Ballesteros et al., 2017).

In the NW of Spain, Picos de Europa is an outstanding location worldwide to study glaciokarst processes and more deeply explore the potential of cave archives as records for paleoenvironmental changes, since Picos de Europa combines outstanding glaciokarst landforms (Smart, 1986) with the largest cluster of deep caves worldwide (Ballesteros et al., 2019a). This study focuses on the Covadonga Lakes and their surroundings, located in the NW of Picos de Europa, a reference location for glacial and karst research (e.g. Rodríguez-Rodríguez et al., 2014; Serrano et al., 2017; Telbisz et al., 2019). Gale and Hoare (1997) and Alonso (1998) elaborated glacial reconstruction studies and Jiménez-Sánchez and Farias (2002) concluded that the local Glacial Maximum (local GM) took place ca. 20 ka before the global LGM, proposing a subsequent phase of generalized glacier retreat. Later, Moreno et al. (2010) established the regional paleoenvironmental evolution since 38 ka based on the

Enol Lake record and geomorphological evidence, and Jiménez-Sánchez et al. (2013) refined the age of the local GM at ca. 45 ka. Likewise, Nieuwendam et al. (2016) studied periglacial processes during late MIS 3 and Ruiz-Fernández et al. (2016) reconstructed the timing of the last deglaciation. Regarding to karst studies, Ballesteros et al. (2015, 2017, 2019b) defined the Quaternary landscape evolution of the area based on cave geomorphology and geochronology.

Nevertheless, the environmental evolution of the Covadonga Lakes area before 45 ka remains mostly unknown, especially regarding to ancient fauna that remains virtually unexplored. The present study is focused on the karst cave named Hayéu l'Osu with the aim to establish the paleoenvironmental evolution of the Western Massif of Picos de Europa during MIS 5c–3. To achieve this goal, we carried out a multidisciplinary work combining glacial reconstruction based on field evidence, speleothem U-Th dating, cave detrital sediment analyses and OSL dating, and the identification of micro- and macromammal remains dated by AMS radiocarbon.

2. SETTING

Picos de Europa National Park (NW of Spain) is a high mountainous area up to 2650 m above sea level (asl), located in the northern slope of the Cantabrian Mountains (Figure 1). Picos de Europa is divided in three massifs (Western, Central and Eastern) by deep fluvial gorges. The main rocks that crop out are Carboniferous limestone and, secondly, Ordovician, Carboniferous and Permian–Triassic sandstone and shale (Merino-Tomé et al., 2013). The climate of Picos de Europa is humid and temperate with fresh summers and without a dry season (Dfb and Dfc following the Köppen classification). The annual precipitation ranges from 1000 to 1800 mm and is distributed throughout the year, whilst the average air temperature ranges between -3 and 17ºC. Snow is present around 6–9 months per year above 1500 m altitude.

Picos de Europa is one of the most relevant karst areas worldwide, since it contains 14% of the deepest caves (>1 km deep) in the world (Ballesteros et al., 2019a). The karst evolution was controlled by river incision and past glaciations (Smart, 1986). Fluvial incision created narrow gorges up to 2 km in depth, conditioning the development of at least 3700 caves summing a total documented length of 420 km, which were most likely formed during the Pliocene and Quaternary (Figure 1C; Ballesteros et al., 2015, 2019b). Cave detrital infill came from the erosion of the above-mentioned nearby bedrock outcrops (Fernández-Gibert et al., 2000; Smart 1986). During the Upper Pleistocene, glaciers reached their local GM extent, occupying ca. 190 km^2 and with their fronts descending down

to 600–900 m altitude (Figure 1C; Serrano et al., 2017). In the study area (Figure 2) glaciers flowed below 1300 m altitude in the surroundings of Covadonga Lakes around 109–95 ka (MIS 5d–c) leading to slackwater sedimentation in caves (Ballesteros et al., 2017). Later, glacial fronts reached at least 900 m altitude (Gale and Hoare, 1997; Alonso 1998; Moreno et al., 2010), defining a local maximum at 45 ± 3 ka (Jiménez-Sánchez et al., 2013). Glacier fronts retreated since ca. 45 ka, being already located at ca. 1000 m elevation at 39 ka, coeval to the development of the Covadonga Lakes (Moreno et al., 2010; Nieuwendam et al., 2016). According to these authors, this retreat continued during MIS 3, taking place under cold, dry and open conditions until 18 ka, coeval with the occurrence of periglacial processes recorded by the Belbin kame deposit (Figure 2; Ruiz-Fernández et al., 2016). Nevertheless, sporadic forest surrounded Picos de Europe during MIS 3 (Uzquiano et al., 2016). Finally, an advance of the glacier front up to similar altitudes than the local maximum is reported at ca. 23–19 ka, which is ascribed to the global LGM (Ruiz-Fernández et al., 2016; Serrano et al., 2017).

3. METHODOLOGY

The methodology combines geomorphological, paleontological and geochronological analyses, including: (1) paleo-glacier reconstruction; (2) cave geomorphology; (3) paleontological identification of the remains, (4) speleothem U-Th dating, (5) detrital cave sediment OSL dating, and (4) radiocarbon dating of macromammal remains. All the spatial information was managed using the Geographical Information System ArcGIS (ESRI), involving topographic contours, orthophotographies and topographic digital models from the Spanish National Institute of Geography (www.cnig.es; last access on April 2019).

3.1 Paleo-glacier reconstruction

Paleo-glacier topography was reconstructed in the study area (Figure 2) for the local GM stage based on geomorphological evidence compiled in Ballesteros et al. (2015, 2019b) and bed topography information. Terminal moraines, glacial arêtes and cirques were used to infer the location of former glacier margins during the local GM stage. Glacier topography was interpolated from 25 theoretical ice surface profiles reconstructed comprising the routing pathways followed by glacier tongues along the valleys and inferred from geomorphological indicators of glacier flow direction. Theoretical ice surface profiles were adjusted following the methods explained in Benn and Hulton (2010), using the GlaRe toolbox for ArcGIS (Pellitero et al., 2016). Basal shear stress values up to 80–120 KPa were needed to

adjust the theoretical ice surface profiles to existing geomorphological evidence, which are consistent with those observed in modern glaciers (50 to 150 KPa; Pellitero et al., 2016). The shape factor of the valley was calculated for 62 cross sections to account for the topographic controls of glacial valley shape on the basal shear stress. Once reconstructed, the digital elevation model of the former glacier topography was used to estimate the Equilibrium Line Altitude (ELA) in steady-state conditions through the Area Altitude Ratio Balance Ratio (AABR) method of Osmaston (2005) using the ELA toolbox (Pellitero et al., 2015). We consider a range of balance ratio values of 1.9 ± 0.8 representative for maritime glacier datasets (Rea, 2009).

3.2 Cave geomorphology

We studied the geomorphology of Hayéu l'Osu Cave in order to establish its development and its sedimentary infill. To achieve this, we carried out the topographic survey in collaboration with speleological groups and the geomorphological mapping of the cavity at 1:100 scale. The cave survey and geomorphological map were developed in ArcGIS following the procedure described in Ballesteros et al. (2015). The cave survey was delineated by means of 569 stations distributed along the cave conduits and 608 measurements of distance, direction and inclination between stations using a DistoX rangefinder, including the vertical and horizontal diameter of the conduit at each station. These measurements were analyzed using the Compass software. Later, the geomorphological map was drawn projecting cave forms and deposits on the cave survey.

3.3 Paleontological analyses

To search for micromammal remains, four samples of detrital sediments (named HAY-07, HAY-08, HAY-09 and HAY-10) summing up to ~90 kg were collected from alluvial sequences of Hayéu l'Osu Cave.. Samples were water-screened using two superimposed sieves of 2- and 0.5-mm mesh size. Sieves were not previously used preventing hypothetic contamination from previous samples in the laboratory. Fine sieved samples was examined using a parallel-optics type stereo microscope Nikon SMZ800N under 10x magnification. Photographs were taken with a 5 Mpx resolution digital camera, and image orientation correction was done with Adobe Photoshop CC software. We used teeth samples of current fauna as a comparison material to identify the micromammal remains found in the study cave. The reference material used belongs to *Arvicola monticola*, *Microtus lavernedii, Microtus lusitanicus* and *Clethrionomys glareolus*, all of them collected from *Tyto alba* pellets in the Cantabrian

Region, as well as MIS 3 fossil material of *Pliomys coronensis* (=*P. lenki*) recovered from the nearby archeological site of La Güelga Cave (Figure 1C).

Macromammals were discovered by speleologists from Grupo Espeléologico Polifemo (Oviedo) and collaborators. Macro remains were recovered using the archaeological methodology, mapping their occurrence on the geomorphological map (section 3.2). These remains were prepared for taxonomic and taphonomic analyses by removing physically the silt and clay attached to the bones and consolidating the samples with Paraloid B-72. Finally, we calculated the Minimum Number of Individuals (MNI) of each species taking into account each skeletal element. The fossils are stored in the Department of Geology at the University of Oviedo (Spain).

3.4 U-Th dating

Three flowstone samples from the study cave were dated by U decay series. Supplementary Data (Figure S1) includes the geomorphological sections of the sampled flowstones. All samples were collected in-situ with the aid of a hammer and a chisel, and drilled in the laboratory using a hand drill to extract 0.1-0.2 g of carbonate powder, which was treated and analyzed at the Xi'an Jiaotong University (China), following the procedures described in Edwards et al. (1987). Each sample was dissolved with HNO_3 and spiked with a ^{229}Th – ^{233}U – ^{236}U carrier solution. Once the Fe solution and the ammonium hydroxide is added, the separation of U and Th was carried out using column chromatography with an anion exchange resin. Finally, U and Th fractions were analyzed in a multicollector-inductively coupled plasma mass spectrometer (MC-ICP-MS) ThermoFisher Neptune Plus using U decay constants reported in Cheng et al. (2013). The ages are expressed in years before present (BP) with their 2σ uncertainty.

3.5 OSL dating

Optically stimulated luminescence (OSL) dating was applied to date endokarst detrital sediments. We collected five samples from sandy layers recognized in the cave stratigraphic sections detailed in Supplementary Data (Figure S2). Samples were taken driving opaque PVC tubes (550 mm diameter, 4 mm wall) in sandy material and then carefully covered with aluminum foil immediately after extraction. Samples were processed in the luminescence laboratory of the Institute of Geology Isidro Parga Pondal, University of A Coruña (Spain). Under red light conditions, sand materials stored within the tubes were dried and sieved. The grain fraction 180–250 µm was dried at 45°C and treated with

HCl and H_2O_2 in order to remove carbonates and organic matter, respectively, which constituted 65–90% of the samples. Furthermore, a centrifugation step adding a high-density solution was needed to separate quartz from feldspar and heavy minerals. Later, a HF dilution was used on the quartz-rich fraction to obtain pure quartz. Infrared Stimulated Luminescence (IRSL) was used to verify quartz purity at the end of sample treatment.

OSL signals were recorded using an automated RISØ TL/OSL-DA-15 reader equipped with a photomultiplier EMI 9635 QA (PMT) and a $^{90}Sr/^{90}Y$ source (dose of 0.120 ± 0.003 $Gy \cdot s^{-1}$). An optical 6 mm-thick Hoya U-340 filter was placed between the aliquots and the PMT to measure the UV range emission. The Single Aliquot Regeneration (SAR) protocol (Murray and Wintle, 2000) was applied on multigrain aliquots to estimate the equivalent Dose (D_e), considering the Central Age Model (Galbraith et al., 1999) to date each sample. Frequency histograms of D_e of samples HAY-07, 09, 10 and 11 are included in Supplementary Data (Figure S3). Sample HAY-08 is not included because of its low reliability (only 4 aliquots) but its age is consistent with other OSL datings. Preheat tests were previously performed and dose recovery tests used on bleached aliquots (Murray and Wintle, 2003).

The activity concentration of radioisotopes (^{40}K, and ^{238}U, ^{235}U and ^{232}Th decay chains) was estimated using low background gamma-ray spectrometry. Measurements of calcined and grinded sediments were performed in a coaxial Canberra XTRA gamma detector (Ge Intrinsic) model GR6022 within a 10 cm-thick lead shield. The alpha dose-rate was neglected due to the HF etching step, and the beta dose-rate corrected (Brennan, 2003). The cosmic dose-rate was estimated following Prescott and Hutton (1994) and using the conversion factors proposed by Guerin et al. (2011). Resultant OSL ages are expressed in years before present (BP) with their corresponding 2σ uncertainty.

3.6 Radiocarbon dating

Two samples from macromammal bones were sampled for radiocarbon dating through accelerator mass spectrometry (AMS). Radiocarbon measurements (reference order 13274/18) were performed at the Poznan Radiocarbon Laboratory, Poland. The obtained ages were calibrated using the software OxCal v.4.3.2 (Bronk Ramsey, 2017) against the INTCAL 13 curve (Reimer et al., 2013), considering the 2σ standard deviation (95.4% probability). The calibrations are included in Supplementary Data (Figure S4) and calibrated dates are expressed in cal ka BP.

4. RESULTS

4.1 Paleo-glacier reconstruction

Glaciers formed an ice field in the surroundings of Covadonga Lakes during the local GM, occupying a total surface extent of 36.18 km^2 and covering the entrance of Hayéu l'Osu Cave (Figure 3). Glacier tongues reached total lengths of ca. 2 km along the valleys of Ordiales, Hunhumia, and Pomperi; up to 9.5 km along El Bricial–Vega de Enol valleys; 5.9 km along Ercina valley; and 6.6 km along the former Belbín glacier. Glacier fronts were placed at ca. 1040 m altitude in the Ordiales, Hunhumia and Ercina valleys; 925–1030 m in the El Bricial–Vega de Enol valleys; and 810 m in Belbín (Figure 3). Glacier maximum thickness reached up to 105-220 m along the El Bricial–Vega de Enol valleys, 170 m along the Belbín flow line, 170 m along Ercina valley, and between ca. 114 and 168 m along the valleys Ordiales, Hunhumia, and Pomperi. The steady-state ELA was most likely set at 1524 ± 36 m (Figure 3).

4.2 Cave geomorphology

The Hayéu l'Osu Cave is mainly formed by a 1.6 km-long conduit (named Stream Gallery) slightly tilted towards the SE, and by vertical conduits summing up to 135 m in depth (Figure 4A). Vertical conduits connect the Stream Gallery and the topographic surface as shown in the cave longitudinal profile (Figure 4B). Geomorphological evidence includes alluvial deposits, breakdown deposits, speleothems and slackwater deposits. Alluvial sediments up to 3 m thick are present along the Stream Gallery (Supplementary Data, Figure S2), involving active channel and terrace deposits. Active channel deposits are located along the cave stream (Figure 4C) and resulted from the erosion of terrace deposits placed at the bottom and walls of the NW of the study cave (Figures 4D and 5A–E). Terrace deposits are perched up to 20 m above the streambed and are occasionally covered by flowstones and stalagmites (Figure 4E). Active channel deposits and most terrace deposits are grain-supported and contain sub-angular to rounded calcareous pebbles and cobbles, containing no matrix or with 5-20% of sandy matrix (70–85% of carbonate and 15–30% of quartz). Both deposits comprise also sub-rounded allochthonous pebbles and cobbles of sandstone, bauxite and diabase. In addition, alluvial sand (70–95% of carbonate and 5–30% of quartz) form also minor terraces or constitute layers interbedded within the pebble and cobble deposits. These sand deposits may eventually contain micromammal remains, which have been identified and described in detail in section 4.3. Breakdown deposits are common along the study cave, including angular calcareous boulders less than 2 m in diameter formed by rock fall processes. Regarding the speleothems, they commonly appear in cave

passages perched above the cave stream. Flowstone up to 3 m thick and stalagmites less than 2 m height occasionally precipitated on top of alluvial and breakdown deposits, however, flowstones covered by sandy terrace deposits were also recognized. Finally, slackwater deposits show 0.5–3 m of laminated silt and clay (Figure 4F) deposited essentially in the central part of the study cave (Figure 4A). These deposits would be related to cave floods similar to what has been observed in the nearby Torca La Texa shaft (Figure 2; Ballesteros et al., 2017).

4.3 Paleontology of mammal bones

Seven fragments of arvicoline molars and one fragment of a rodent incisor were found in samples from HAY-7, 8 and 9, collected in the Stream Gallery (Figure 4A). These remains show dentine removal by erosion and four of them show also rounded edges. The best-preserved fragment corresponds to a complete enamel prism found in sample HAY-9. When comparing this fragment with the upper first molars of extinct and living arvicolines from the Cantabrian Region (Figure 5), its size and angle in occlusal view (Figure 5a') matches with the morphology of an upper first or second molar (Figure 5b'–e'). The curvature of the anterior side of the triangle at the tooth's base indicates that it belongs to a rooted molar (Figure 5a''), clearly different respect to ever-growing molars (Figure 5D, E and F). All these mentioned morphological features and the absence of curvature at the basal part of the posterior side of the prism (Figure 5a''), match with the morphology of the buccal salient angle 3 (BSA3) of the first upper molar (M^1). Among the arvicolines from the Upper Pleistocene of the Iberian Peninsula, only two species bear rooted molars. One of them is *P. coronensis* (Figure 5B), a very common vole in rocky environments during MIS 3 and earlier before its extinction during MIS 2 in the Cantabrian Region, territory that constituted the last refuge for this species before its complete disappearance (Cuenca-Bescós et al., 2010). The other rooted-molar species is *C. glareolus* (Figure 5C), which currently inhabits the well-developed forests of the Cantabrian Region and other Eurasian areas, but which is absent in alpine environments. Considering the compared morphology and the chronological context (defined in section 4.4), the enamel fragment of HAY-9 has been ascribed to the species *P. coronensis*. There is another enamel fragment at HAY-7 whose morphological features at its basal part indicate it belongs to a rooted molar, but no further identification can be done due to its poor preservation.

A total amount of 81 macromammal remains, all of them corresponding to small-sized bovids, were recovered from two sites named Llamaeyu and Stream galleries (Figure 4). In Llamaeyu Gallery, radius, metacarpals, phalanxes, skull fragments, vertebras, ribs, one molar and other bones were found without anatomic connection on top of a breakdown deposit (Figure 6A) whereas, in the Stream Gallery, a scapula was located on a detrital deposit (Figure 6B). Morphology and morphometry of teeth and skeletal elements are distinctive of chamois (Figure 7), so they are ascribed to *Rupicapra pyrenaica* (a comprehensive discussion about the specific attribution of Upper Pleistocene chamois from the Iberian Peninsula is provided by Álvarez-Lao, 2014). This fossil assemblage corresponds to a minimum of four individuals (MNI): two young and two adults. The lack of anthropic activity signs excludes humans as responsible for the bone accumulation. In general, no carnivore marks are detected, suggesting that the bone accumulation was related to a natural trap. Only one bone shows teeth marks (Figure 7D) produced by a small carnivore, most likely due to scavenging rather than predation. In addition, only one bone (corresponding to one of the young individuals) shows erosion features due to transportation by water (Figure 7C). From an environmental perspective, occurrence of *R. pyrenaica*, a typical alpine ungulate, at Hayéu l'Osu Cave is consistent with the current rocky mountain landscape of the area. Moreover, presence of a herbivore mammal in this cave clearly indicates ice-free conditions in the near surroundings during the time they lived (Álvarez-Lao, 2014).

4.4 Geochronology

Three speleothem samples from the study cave were analyzed using U-Th dating (Table 1). Samples exhibit ^{238}U content lower than 100 ppb and high initial $\delta^{234}U$ (1000-3000 ppm). Standard procedures to correct the ages assume an initial $^{230}Th/^{232}Th$ atomic ratio of $4.4 \pm 2.2 \cdot 10^{-6}$ (Edwards et al., 1987; Cheng et al., 2013) and the obtained ages are considered reliable.. Sample HAY-12 (263 ± 18 ka) corresponds to the base of an overturned set of flowstones and stalagmites, originally precipitated on top of slackwater deposits (Figure 8A). The age provided for HAY-12 represents a minimum age for the slackwater deposits, which would have been decanted by cave flooding before 263 ± 18 ka, during the Middle Pleistocene. Subsequently, the slackwater deposits were eroded causing the collapse of the overlying flowstones and stalagmites. Similarly, samples HAY-06 (132 ± 1 ka) and HAY-13 (135 ± 7 ka) have precipitated fossilizing fluvial deposits (Figure 8B and C), which were eroded later in the case of HAY-06. Both datings indicate the occurrence of a first alluvial sequence older than 135-132 ka, probably during MIS 6.

In the study cave, five alluvial deposits described in section 4.2 were dated using OSL from 84 ± 10 to 36 ± 3 ka (Table 2, Figure 8C-G). The estimated dose-rates were very low due to the low radioisotope content, being below 1 Gy ka^{-1} for most samples. No disequilibrium is observed in the U and Th decay chains. The OSL signals were dim but fast, and provided poor signal to background ratios, causing the rejection of a high number of aliquots, being the number of accepted aliquots between 4 and 35. The D_e distributions were non-skewed and the over dispersion (Table 2) of the mean of the Central Age Model was low, showing no evidence of incomplete bleaching of the alluvial sand grains before they were introduced into the cave. Thus, the Central Age Model was used for assessing the OSL ages. After bleaching, the quartz was for a short period on the topographical surface before being introduced into the study cave. We consider this time to be short since the study cave is located in a hill that probably acted as a by-pass area to lower zones where widespread glacial and fluvioglacial sedimentation took place (Figures 2 and 3). However, reworking processes are not totally discarded. The chronological framework provided allows us to define two alluvial sequences occurring after the first alluvial sequence identified by U-Th dates. According to this, a second alluvial sequence corresponds to terrace sediments deposited between 84 ± 10 and 65 ± 16 ka, ranging from MIS 5c to MIS 4 (Figure 8C-F), while a third sequence includes a fluvial terrace formed at 36 ± 3 ka during MIS 3a (Figure 8G).

The chronology of the second and third alluvial sequences provides the chronological framework of the arvicolinae remains, while the radiocarbon dates represent the timing of the chamois. A fragment of metatarsal from Llamaeyu Gallery has an AMS ^{14}C age of 36 ± 1 cal ka BP whilst the scapula recovered in Stream Gallery provided an age of 34.5 ± 0.6 cal ka BP (Table 3).

5. DISCUSSION: PALEOENVIRONMENTAL EVOLUTION

Cave geomorphology and U-Th ages provide new data about the origin and evolution of the Hayéu l'Osu Cave during the Middle Pleistocene (Figure 9). Flowstone ages suggest that the cave was formed prior to 263 ka (Figure 9A), like most karst cavities studied in Picos de Europa (Smart, 1986; Ballesteros et al., 2015, 2019). Since its origin, Hayéu l'Osu Cave has undergone inundations that would be related to Middle Pleistocene glaciations, followed by speleothem precipitation at 263 ± 18 ka (MIS 8). Other studies have documented coeval breccia cementation in surficial talus deposits in Puertos de Áliva (Villa et al., 2013), between the Central and Eastern massifs of Picos de Europa (Figure 1C). Later, at the end of MIS 6, flowstone precipitation took place in the cave at 135-132 ka,

covering the first alluvial sequence previously deposited. All these speleothems and detrital sediments partially filled the Hayéu l'Osu Cave, as occurred in other nearby caves named Pozu Llucia and Torca La Texa (Figure 2; Ballesteros et al., 2019).

The paleoenvironmental evolution of the surroundings of Covadonga Lakes during MIS 5c-3 is established based on the combination of geomorphological-stratigraphical and paleontological data and kernel density functions (Figure 10) of U-Th, OSL and radiocarbon ages obtained in the cave. This probability analysis considered also previous datings carried out in Enol lacustrine sediments by Moreno et al. (2010) and in Vega de Comeya border polje by Jiménez-Sánchez et al. (2013). Four phases have been distinguished (Table 4 and Figure 11) according to the probabilistic distribution of Figure 10.

5.1 Phase 1 (98-60 ka; MIS 5c–4)

The first phase described for the study area ranges between ca. 98 and 60 ka (Figure 11A). After glacial advances recorded during MIS 5cd, dated in the Central Cantabrian Mountains at 114 ± 7 ka based on *in situ* produced cosmogenic nuclide ^{10}Be (Figure 1B; Rodríguez-Rodríguez et al., 2016), a glacial retreat episode occurred in the study area during MIS 5c-4. In Hayéu l'Osu Cave this episode might correspond to the sedimentation of the second alluvial sequence that includes *P. coronensis*. Alluvial deposits are dominated by carbonate sand and silt (section 4.2), coming from the glacial erosion of Carboniferous limestone, while pebbles and cobbles of sandstone and diabase were eroded from sandstone and igneous dyke outcrops located in higher areas of the Western Massif of Picos de Europa (Ballesteros et al., 2017, 2019b). Thus, the Ercina glacier that flowed from the summit areas elevated more than 2000 m altitude of the Western Massif (Figure 3) eroded the limestone, sandstone and diabase bedrock and transported the resulting sediment load to the glacier fronts located higher than 1400 m altitude (Figure 11A). Sediments were probably transported by glacial meltwater to the surroundings of the study cave, in a fluvioglacial environment inhabited by *P. coronensis*. The roundness of sediment particles observed in the alluvial sequence (section 4.2) as well as in the enamel remains discovered in the study cave (section 4.3) are both compatible with this interpretation. Finally, the presence of *P. coronensis* indicates that bedrock was exposed near the cave under relatively cold conditions, and hence, the glacier advance was less extensive than the local GM extent.

The sediments of the second alluvial sequence might have formed during MIS 5d glaciation identified directly in the central Cantabrian Mountains (Figure 1B; Rodríguez-Rodríguez et al., 2016) and indirectly in the nearby Torca La Texa shaft (Figure 2; Ballesteros et al., 2017). The decantation of glacial origin rhythmite in this shaft (located at 1350 m elevation) at 109-95 ka suggests that the Ercina glacier front was at around 1350-1400 m at the beginning of phase 1.

5.2 Phase 2 (48–42 ka; MIS 3c)

The second phase (Figure 11B) corresponds to the local GM advance of glaciers in the study area. The Vega de Comeya border polje was occupied by a proglacial lake that was being filled by calcareous alluvial deposits from the south-facing slopes of the Western Massif and siliceous alluvial sediments from the north-facing slopes (Jiménez-Sánchez and Farias, 2002). OSL dating yielded a minimum age of 45 ± 3 ka for the onset of glacio-lacustrine sedimentation in the border polje while organic remains from a sand and gravel unit placed immediately on top yielded a radiocarbon age of 44.1 ± 0.9 cal ka BP, constraining the age of the local GM (Jiménez-Sánchez et al., 2013). Similarly, the nearby Belbín kame terrace deposit (Figure 2) yielded a minimum reference age of 36.5 ± 0.5 cal ka BP for the base of its sequence and, hence, for the Belbín moraine deposition (Ruiz-Fernández et al., 2016). The reconstruction of the local GM extent (section 4.1) suggests that glaciers were less extensive compared to previous reconstructions proposed by Gale and Hoare (1997), but it is in agreement with those developed in Alonso (1998), Serrano et al. (2017), and Ruiz-Fernández et al. (2016). The reconstruction also indicates that glacier fronts descended down to –1040–810 m asl, covering the calcareous bedrock where the Hayéu l'Osu Cave develops (Figure 11B), which was located below the estimated ELA (1524 ± 36 m). The altitude of the steady-state ELA in our work is consistent with previous regional ELA reconstructions made by Santos-González et al. (2013), but ca. 100 m lower than the mean ELA estimated in Serrano et al. (2017).

5.3 Phase 3 (42-38 ka; MIS 3b)

Phase 3 represents the onset of glacier retreat in the surroundings of Covadonga Lakes (Jiménez-Sánchez and Farias, 2002). Glacier retreat was recorded by proglacial lacustrine sedimentation at Enol Lake at 38 ± 2 cal ka BP, exposing the glacial depression now occupied by Enol Lake but with the glacial front still located close to the lake and supplying ablation water and coarse inorganic sediments (Moreno et al., 2010). During this phase (Figure 11C), the evolution of the Ercina glacier

front would have been consistent with that of El Bricial-Vega de Enol glacier recording a new episode of detrital sediment infill at 39 ± 3 ka. Hence, the Ercina glacier was likely shorter at ca. 38 ka than previously assumed (Moreno et al., 2010). Glacier retreat prior to 36–39 ka has also been reported in Puertos de Áliva, a site located between the Central and Eastern massifs (Figure 1C; Serrano et al., 2012).

5.4 Phase 4 (37–33 ka; MIS 3a)

Glaciers continued receding during phase 4 (Figure 11D). The Ercina glacier front had already ascended well above 1400 m by 37 ka, while the third alluvial sequence was being deposited within the Hayéu l'Osu Cave. The third detrital sequence is thinner and less extensive than the second detrital sequence, suggesting that the volume of surface sediment was higher during MIS 5d glaciation than during the local GM of MIS 3c. MIS 5d glaciation occurred after the Eemian interglacial substage, when weathering processes would have been more intense than over MIS 4. Besides, the third alluvial sequence deposited at 36 ± 3 ka within the study cave also involved micromammal remains. Consequently, this sequence should come from fluvio-glacial sediments sourcing from the retreating glacier fronts similar to the interpretation for the second alluvial sequence (section 5.1) even if minor reworking processes would take place.

Subsequently, at least three chamois accidentally fell inside the cave. The current position of these remains at 50 and 100 m depth (from the topographic surface) and the absence of evidence produced by carnivores, scavengers or humans support the role of the cave as a natural trap. Only one bone shows minor bite marks caused by a small carnivore (e.g. weasel, beech marten). In the Llamaeyu Gallery, bone remains most likely arrived by gravity processes and minor water transport, as the fauna assemblage is not in anatomic connection and is related to a breakdown deposit (section 4.2). In the Stream Gallery, the chamois bone is located in a subhorizontal conduit and have been transported by an underground stream after its accidental fall in the cave. The lack of transport marks recognized in the bone suggests that it may have arrived protected by the soft parts of the animal.

The existence of chamois bones points to the presence of an alpine environment with exposure of rocky areas developed under relatively cold climate at 37–33 ka. This time range coincides with a relative cold period according to the NGRIP $\delta^{18}O$ ice core record (Figure 12; NGRIP, 2004). Nevertheless, at a regional scale, the presence of chamois is coeval with a period of less cold conditions marked by an increase in organic matter and coarse sediments in the paleolake of Puertos

de Áliva (1400 m altitude) between 36 and 32 ka (Serrano et al., 2012). In lower areas, the pollen record of El Esquilleu Cave (Figure 1C; 350 m asl) revealed the occurrence of *Pinus* forest with minor deciduous and evergreen oaks, but also heathland shrubs in the SW of Picos de Europa at around 38–34 ka (Uzquiano et al., 2016) that would have been part of the chamois diet.

During the late MIS 3, chamois constituted one of the main food sources of the Mousterian–Aurignacian humans who lived in areas below 400 m elevation in the Cantabrian Mountains (Yravedra and Cobo-Sánchez et al., 2015). Around Picos de Europa, archeological excavations discovered abundant remains of hunted chamois in Sopeña (Pinto-Llona et al., 2012), El Esquilleu (Uzquiano et al., 2012; Yravedra et al., 2014), La Güelga (Menéndez et al., 2018) and other cavities suggesting that the hunting zones were located in lower areas (Figure 1C). However, the chamois remains found in Hayéu l'Osu Cave indicate that the populations of this caprine could also have occupied areas of Picos de Europa up to, at least, 1400 m elevation, during 37–33 ka.

6. CONCLUSIONS

We propose a new paleoenvironmental evolution model during MIS 5c–3 for Picos de Europa based on a multidisciplinary work combining glacial and cave geomorphology, Quaternary paleontology and geochronology on a glaciokarst area. The study of sediment records in Hayéu l'Osu Cave have allowed us to constrain the timing of glacier retreat, and thus complement previous reconstructions on paleo-glacier evolution in Picos de Europa. In addition, mammal remains preserved in caves are exceptional indicators of glacial ice-free areas in the past, pointing out to a paleoenvironment developed over successive pulses of the glacial evolution.

Three alluvial stratigraphic sequences have been identified in Hayéu l'Osu Cave. The first sequence was deposited before 135-131 ka (MIS 6), while the second and third sequence, with micrommamal remains, were sedimented at 98–60 ka and ca. 36 ka respectively. Additionally, chamois remains (37–33 ka) were found on top of the third sequence. This stratigraphic record suggests the development of alpine ice-free areas at ca. 1400 m altitude during 98-60 ka (MIS 5c–4), when glaciers were probably located at higher altitudes. Later, glaciers with a length of 9.5 km and up to 100-220 m in thickness, descended down to 810–1030 m elevation during the local GM stage, establishing a proglacial lake environment in the Comeya border polje at 48–42 ka (MIS 3c). Over this period, the study cave was located in the glacial ablation zone and covered by glaciers. A general trend of glacier retreat occurred from 42–38 ka, with the glacial fronts located above 1400 m altitude at 37–33 ka. In this setting,

chamois inhabited the ice-free rocky steep slopes of Picos de Europa, in agreement with a slight increase in local temperature.

In addition, the distribution of species in the Cantabrian Region provides further insights on the paleoenvironmetal evolution of the study area. Remains of *P. coronensis* allow us to extend its altitudinal distribution up to ca. 1400 m in the Cantabrian Region during MIS 4, whereas the chamois bone assemblage of Hayéu l'Osu Cave constitutes the oldest evidence of *R. pyrenaica* above 1000 m altitude of the Cantabrian Region. Chamois inhabited the highlands of Picos de Europa at 37-33 ka coevally with human occupation in lower areas, who broadly hunted chamois. However, our outcomes suggest that the studied chamois remains fell accidently in Hayéu l'Osu Cave, being accumulated in the stratigraphic record by natural processes without any human contribution.

AUTHOR CONTRIBUTION

DB, LRR and MJS conducted the research. MMD and LRR elaborated the paleo-glacier reconstruction. DB performed the cave geomorphology and collected all samples in cooperation with PV, IDF and the speleological team. AAV found and identified rodent remains under the guidance of CL, whilst DAL studied the macromammal assemblages. JS carried out the OSL datings, and CPM obtained the U-Th ages under the direction of HC. DB, LRR, DAL, AAV, IDF, PV and CPM wrote the article and designed the figures. All authors have contributed to the discussion.

ACKNOWLEDGEMENTS

Picos de Europa National Park founded this work through the Geocancosta (FC-GRUPIN6IDI/2018/000184) and FUO-300-17 projects, receiving the grateful assistance of the National Park staff and the speleologists from Grupo Espeleológico Polifemo (Oviedo), GES Montañeiros Celtas (Vigo), Grupo de Espeleología Diañu Burlón (Corvera de Asturias), and Espéleo Club Aradelas (Vigo). LRR is grant holder of the post-doctoral Clarín-COFUND Program, financed jointly by the 7th WP of the European Union–Marie Curie Actions and Gobierno del Principado de Asturias (Reference ACA-17-19). We appreciate the work of Jo de Waele, Rafael López-Martínez and other reviewers.

REFERENCES

Adamson, K.R., Woodward, J.C., Hughes, P.D. 2014. Glaciers and rivers: Pleistocene uncoupling in a Mediterranean mountain karst. Quaternary Science Reviews, 94, 28–43.

Alonso, V. 1998. Covadonga National Park (Western Massif of Picos de Europa, NW Spain): a calcareous deglaciated area. Trabajos de Geología 20, 167–181.

Álvarez-Lao, D.J. 2014. The Jou Puerta Cave (Asturias, NW Spain): a MIS 3 large mammal assemblage with mixture of cold and temperate elements. Palaeogeography, Palaeoclimatology, Palaeoecology 393, 1–19.

Audra, P., Quinif, Y., Rochette, P. 2002. The genesis of Tennengerbirge karst and caves (Salzburg, Austria). Journal of Cave and Karst Studies 64, 153–164.

Audra, P., Bini, A., Gabrovšek, F., Häuselmann, P., Hobléa, F., Jeannin, P.Y., Kunaver, J., Monbaron, M., Šušteršič, F., Tognini, P., Trimmel, H., Wildberger, A. 2006. Cave genesis in the Alps between the Miocene and today: a review. Zeitschrift für Geomorphologie 50, 153–176.

Ballesteros, D., Jiménez-Sánchez, M., Giralt, S., García-Sansegundo, J., Meléndez-Asensio, M. 2015. A multi-method approach for speleogenetic research on alpine karst caves. Torca La Texa shaft, Picos de Europa (Spain). Geomorphology 247, 35–54.

Ballesteros, D., Jiménez-Sánchez, M., Giralt, S., DeFelipe, I., García-Sansegundo, J. 2017. Glacial origin for cave rhythmite during MIS 5d–c in a glaciokarst landscape, Picos de Europa (Spain). Geomorphology 286, 68–77.

Ballesteros, D., Fernández-Martínez, E., Carcavilla, L., Jiménez-Sánchez, M. 2019a. Karst Cave Geoheritage in Protected Areas: Characterisation and Proposals of Management of Deep Caves in the Picos de Europa National Park (Spain). Geoheritage 11(4), 1919-1939..

Ballesteros, D., Giralt, S., García-Sansegundo, J., Jiménez-Sánchez, M. 2019b. Quaternary regional evolution based on karst cave geomorphology in Picos de Europa (Atlantic Margin of the Iberian Peninsula). Geomorphology 336, 133–151.

Benn, D.I., Hulton, N.R.J. 2010. An ExcelTM spreadsheet program for reconstructing the surface profile of former mountain glaciers and ice caps. Computers & Geosciences 36, 605–610.

Bočić, N., Faivre, S., Kovačić, M., Horvatinčić, N. 2012. Cave development under the influence of Pleistocene glaciation in the Dinarides – an example from Štirovača Ice Cave (Velebit Mt., Croatia). Zeitschrift für Geomorphologie, 56, 409–433.

Bronk Ramsey, C. 2017. Methods for Summarizing Radiocarbon Datasets. Radiocarbon 59, 1-25.

Brennan, B.J. 2003. Beta doses to spherical grains. Radiation Measurements 3, 299–303.

Cheng, H., Edwards, L. R., Shen, C.-C., Polyak, V.J., Asmerom, Y., Woodhead, J.,Hellstrom, J., Wang, Y., Kong, X., Spötl, C., Wang, X., Alexander, E. C. 2013. Improvements in 230Th dating, ^{230}Th and ^{234}U half-life values, and U-Th isotopic measurements by multi-collector inductively coupled plasma mass spectrometry. Earth and Planetary Science Letters, 371-372, 82-91.

Clark, P.U., Dyke, A.S., Shakun, J.D., Carlson, A.E, Clark, J., Wohlfarth, B., Mitrovica, J.X., Hostetler, S.W., McCabe, A.M. Science 7, 710-714.

Colhoun, E.A., Kiernan, K., Barrows, T.T., Goede, A. 2010. Advances in Quaternary studies in Tasmania. Special Publications, 346. Geological Society of London. Londres. 165–183.

Cuenca-Bescós, G., Straus, L. G., García-Pimienta, J. C., González Morales, M.R., López-García, J.M. 2010. Late Quaternary small mammal turnover in the Cantabrian Region: The extintion of *Pliomys lenki* (Rodentia, Mammalia). Quaternary International 212, 129–136.

Edwards, R.L., Chen, J.H., Wasserburg, G.J. 1987. ^{238}U, ^{234}U, ^{230}Th, ^{232}Th systematics and the precise measurement of time over the past 500,000 years. Earth and Planetary Science Letters, 81, 175–192.

Fernández-Gibert, E., Calaforra, J.M., Rossi, C. 2000. Speleogenesis in the Picos de Europa Massif, Northern Spain, in: Klimchouk, A., Ford, D., Palmer, A., Dreybrodt, W. (Eds.), Speleogenesis: Evolution of Karst Aquifers, National Speleological Society, Huntsville, Alabama, pp. 352–357.

Ford, D.C. 1971. Characteristics of Limestone Solution in the Southern Rocky Mountains and Slekirk Mountains, Alberta and British Columbia. Canadian Journal of Earth Sciences 8, 585–609.

Ford, D.C. 1979. A review of alpine karst in the southern Rocky Mountains of Canada. National Speleological Society Bulletin 41, 53–65.

Galbraith, R.F., Roberts, R.G., Laslett, G.M., Yoshida, H., Olley, J.M. 1999. Optical dating of single and multiple grains of quartz from Jinmium Rock Sherlter, Northern Australia: Part 1, Experimental design and statistical models. Archaeometry 41, 339–364.

Gale, S.J., Hoare, P.G. 1997. The glacial history of the northwest Picos de Europa of northern Spain. Zeitschrift für Geomorphologie 41, 81–96.

Glover, R. R. 1977. A conceptual model of cave development in a glaciated region. Proceedings of 7th International Speleological Congress. International Union of Speleology, Sheffield, pp. 220–221.

Guerin, G., Mercier, N., Adamiec, G. 2011. Dose-rate conversion factors: update. Ancient TL 29, 5–8.

Häuselmann, P. 2013. Large epigenic caves in high-relief areas. In: Shroder, J., Frumkin, A. (Eds.) Treatise on Geomorphology, Vol 6, Karst Geomorphology. Academic Press, San Diego, 207–219.

Häuselmann, P., Granger, D.E., Jeannin, P.Y., Lauritzen, S.E. 2007. Abrupt glacial valley incision at 0.8 Ma dated from cave deposits in Switzerland. Geology 35, 143–146.

Isola, I., Ribolini, A., Zanchetta, G., Bini, M., Regattieri, E., Drysdale, R. N., Hellstrom, J.C., Bajo, P, Montagna, P., Pons-Branchu, E. 2019. Speleothem U/Th age constraints for the Last Glacial conditions in the Apuan Alps, northwestern Italy. Palaeogeography, Palaeoclimatology, Palaeoecology 518, 62–71.

Jiménez-Sánchez, M., Farias, P. 2002. New radiometric and geomorphologic evidences of a last glacial maximum older than 18 ka in SW European mountains: the example of Redes Natural Park (Cantabrian Mountains, NW Spain). Geodinamica Acta 15, 93–101.

Jiménez-Sánchez, M., Rodríguez-Rodríguez, L., García-Ruiz, J.M., Domínguez-Cuesta, M.J., Farias, P., Valero-Garcés, B., Moreno, A., Rico, M., Valcárcel, M. 2013. A review of glacial geomorphology and chronology in northern Spain: Timing and regional variability during the last glacial cycle. Geomorphology 196, 50–64.

Lechleitner, F.A., Amirnezhad-Mozhdehi, S., Columbu, A., Comas-Bru, L., Labuhn, I., Pérez-Mejías, P., Rehfeld, K. 2018. The Potential of Speleothems from Western Europe as Recorders of Regional Climate: A Critical Assessment of the SISAL Database. Quaternary 1 (3), 30.

Menéndez, M., Álvarez-Alonso, D., Andrés-Herrero, M. de, Carral, P., García-Sánchez, E., Jordá-Pardo, J.F., Quesada, J.M., Rojo, J. 2018. The Middle to Upper Paleolithic transition in La Güelga cave (Asturias, Northern Spain). Quaternary International 474, 71–84.

Merino-Tomé, O., Suárez Rodríguez, A., Alonso, J., González Menéndez, L., Heredia, N., Marcos, A. 2013. Mapa Geológico Digital continuo E. 1:50.000, Principado de Asturias (Zonas: 1100–1000–1600) [WWW Document]. GEODE. Mapa Geológico Digital Continuo de España. SIGECO-IGME. URL http://cuarzo.igme.es/sigeco/default.htm

Moreno, A., Valero-Garcés, B.L., Jiménez-Sánchez, M., Domínguez-Cuesta, M.J., Mata, M., Navas, A., González-Sampériz, P., Stoll, H., Farias, P., Morello, M., Corella, J., Rico, M. 2010. The last deglaciation in the Picos de Europa National Park (Cantabrian Mountains). Journal of Quaternary Sciences 25, 1076–1091.

Murray, A.S., Wintle, A.G. 2000. Luminescence dating of quartz using an improved single-aliquot regenerative-dose protocol. Radiation Measurements 32, 57–73.

Murray, A.S., Wintle, A.G. 2003. The single aliquot regenerative dose protocol: Potential for improvements in reliability. Radiation Measurements 37, 377–381.

Mylroie, J.E. 1984. Pleistocene climatic variation and cave development: Norsk Geografisk Tidsskrift 38, 151–156.

Mylroie, J.E., Mylroie, J.R. 2004. Glaciated karst: how the Helderberg plateau revised the geological perception. Northeastern Geology and Environmental Sciences 26, 82–92.

Nieuwendam, A., Ruiz-Fernández, J., Oliva, M., Lopez, V., Cruces, A., Freitas, M. da C. 2015. Postglacial landscape changes and cryogenic processes in Picos de Europa (northern Spain) reconstructed from geomorphological mapping and microstructures on quartz grains. Permafrost and Periglacial Processes 27, 96–108.

NGRIP members 2004. High-resolution record of Northern Hemisphere climate extending into the last interglacial period. Nature 431, 147–151.

Osmaston H. 2005. Estimates of glacier equilibrium line altitudes by the Area×Altitude, the Area×Altitude Balance Ratio and the Area×Altitude Balance Index methods and their validation. Quaternary International 138–139, 22–31.

Pellitero, R., Rea, B.R., Spagnolo, M., Bakke, J., Ivy-Ochs, S., Lukas, S., Ribolini, A. 2015. A GIS tool for automatic calculation of glacier equilibrium-line altitudes. Computers & Geosciences 82, 55–62.

Pellitero, R., Rea, B.R., Spagnolo, M., Bakke, J., Ivy-Ochs, S., Frew, C.R., Hughes, P., Ribolini, A., Lukas, S., Renssen, H. 2016. GlaRe, a GIS tool to reconstruct the 3D surface of palaeoglaciers. Computers & Geoscience 94, 77–85.

Pinto-Llona, A.C., Clark, G., Karkanas, P., Blackwell, B., Skinner, A.R., Andrews, P., Reed, K., Miller, A., Macías-Rosado, R., Vakiparta, J. 2012. The Sopeña Rockshelter, a New Site in Asturias (Spain) bearing evidence on the Middle and Early Upper Palaeolithic in Northern Iberia. Munibe (Antropologia-Arkeologia) 63, 45–79.

Plan, L., Filipponi, M., Behm, M., Seebacher, R., Jeutter, P., 2009. Constraints on alpine speleogenesis from cave morphology — A case study from the eastern Totes Gebirge (Northern Calcareous Alps, Austria). Geomorphology 106, 118–129.

Prescott, J.R., Hutton, J.T. 1994 Cosmic ray contributions to dose rates for luminescence and ESR dating: large depths and long term variations. Radiation Measurements 23, 497–500.

Railsback, L.B., Gibbard, P.L., Head, M.J., Voarintsoa, N.R.G., Toucanne, S. 2015. An optimized scheme of lettered marine isotope substages for the last 1.0 million years, and the climatostratigraphic nature of isotope stages and substages. Quaternary Science Reviews 111, 94–106.

Rea, B.R. 2009. Defining modern day Area-Altitude Balance Ratios (AABRs) and their use in glacier-climate reconstructions. Quaternary Science Review 28, 237–248.

Reimer, P., Bard, E., Bayliss, A., Beck, J.W., Blackwell, P., Ramsey, C.B., Buck, C., Cheng, H., Edwards, R.L., Friedrich, M., Grootes, P.M., Guilderson, T.P., Haflidason, H., Hajdas, I., Hatt_e, C., Heaton, T.J., Hoffmann, D.L., Hogg, A.G., Hughen, K., Kaiser, K.F., Kromer, B., Manning, S.W., Niu, M., Reimer, R.W., Richards, D.A., Scott, E.M., Southon, J., Staff, R.A., Turney, C.S.M., Van der Plicht, J. 2013. Intcal13 and Marine13 radiocarbon age calibration curves 0–50,000 years cal BP. Radiocarbon 55, 1869–1887.

Rodríguez-Rodríguez, L., Jiménez-Sánchez, M., Domínguez-Cuesta, M.J., Aranburu, A. 2014. Research history on glacial geomorphology and geochronology of the Cantabrian Mountains, north Iberia (43–42°N/7–2°W). Quaternary International 364, 6–21.

Rodríguez-Rodríguez, L., Jiménez-Sánchez, M., Domínguez-Cuesta, M.J., Rinterknecht, V., Pallàs, R., Bourlès, D. 2016. Chronology of glaciations in the Cantabrian Mountains (NW Iberia) during the Last Glacial Cycle based on in situ-produced 10Be. Quaternary Science Reviews 138, 31–48.

Ruiz-Fernández, J., Oliva, M., Cruces, A., Lopes, V., Freitas, M. da C., Andrade, C., García-Hernández, C., López-Sáez, J.A., Geraldes, M. 2016. Environmental evolution in the Picos de Europa (Cantabrian Mountains, SW Europe) since the Last Glaciation. Quaternary Science Reviews 138, 87–104.

Santos-González, J., Redondo-Vega, J.M., González-Gutiérrez, R.B., Gómez-Villar, A. 2013. Applying the AABR method to reconstruct equilibrium-line altitudes from the last glacial maximum in the Cantabrian Mountains (SW Europe). Palaeogeography, Palaeoclimatology, Palaeoecology 387, 185–199.

Serrano, E., González-Trueba, J.J., González-García, M. 2012. Mountain glaciation and paleoclimate reconstruction in the Picos de Europa (Iberian Peninsula, SW Europe). Quaternary Research 78, 303–314.

Serrano, E., González-Trueba, J.J., Pellitero, R., Gomez-Lende, M. 2017. Quaternary glacial history of the Cantabrian Mountains of northern Spain: a new synthesis, in: Hughes, P.D., Woodward, J.C. (Eds.), Special Publications, 433: Quaternary Glaciation in the Mediterranean Mountains, Geological Society of London, London, pp. 55–85.

Skoglund, R.Ø., Lauritzen, S.E., Gabrovšek, F. 2010. The impact of glacier ice-contact and subglacial hydrochemistry on evolution of maze caves: A modelling approach. Journal of Hydrology 388, 157–172.

Smart, P.L. 1986. Origin and development of glacio-karst closed depressions in the Picos de Europa, Spain. Zeitschrift für Geomorphologie 30, 423–443.

Stuiver, M., Reimer, P.J. 1993. Extended 14C data base and revised CALIB 3.0 14C age calibration program. Radiocarbon 35, 215–230.

Telbisz, T., Tóth, G., Ruban, D.A., Gutak, J.M. 2019. Notable glaciokarst of the World. In: Veress, M. Telbisz, T., Tóth, G., Lózy, D., Ruban, D.A., Gutak, J.M. (Eds), Glaciokarst. Springer, Cham, 373–499.

Tîrlă, L., Drăguşin, V., Bajo, P., Covaliov, S., Cruceru, N., Ersek, V., Hanganu, D., Hellstrom, J., Hoffmann, D., Mirea, I., Sava, T., Sava, G., Şandric, I. In press. Quaternary environmental evolution in the South Carpathians reconstructed from glaciokarst geomorphology and sedimentary archives. Geomorphology, 354: 107038.

Uzquiano, P., Yravedra, J., Ruiz Zapata, B., Gil García, M.J., Sesé, C., Baena, J. 2012. Human behaviour and adaptations to MIS 3 environmental trends (>53–30 ka BP) at Esquilleu cave (Cantabria, northern Spain). Quaternary International 252, 82–89.

Uzquiano, P., Ruiz-Zapata, M.B., Gil-García, M.J., Fernández, S., Carrion, J.S. 2016. Late Quaternary developments of Mediterranean oaks in the Atlantic domain of the Iberian Peninsula: The case of the Cantabrian region (N Spain). Quaternary Science Reviews 153, 63–77.

Villa, E., Stoll, H., Farias, P., Adrados, L., Edwards, R.L., Cheng, H. 2013. Age and significance of the Quaternary cemented deposits of the Duje Valley (Picos de Europa, Northern Spain), Quaternary Research 79, 1-5.

Weremeichik, J., Mylroie, J. 2014. Glacial Lake Schoharie: an investigative study of glaciolacustrine lithofacies in caves, Helderberg Plateau, Central New York. Journal of Cave and Karst Studies 76, 127–138.

Yravedra, J., Gómez-Castanedo, A., Aramendi Picado, J., Baena Preysler, J. 2014. Specialised hunting of Iberian ibex during Neanderthal occupation at El Esquilleu Cave, northern Spain. Antiquity 88, 1035–1049.

Yravedra, J., Cobo-Sánchez, L. 2015. Neanderthal exploitation of ibex and chamois in southwestern Europe. Journal of Human Evolution 78, 12–32.

FIGURE CAPTIONS

Figure 1. (A) Map of the SW of Europe with the location of Picos de Europa (northern Spain). (B) DEM of the N of Spain including the local Maximum Ice Extent (local MIE) recorded by former glaciers in the Cantabrian Mountains (Rodríguez-Rodríguez et al., 2014). (C) DEM of the three massifs of Picos de Europa with the position of the study cave (named Hayéu l'Osu) in the surroundings of Covadonga Lakes (Enol and Ercina lakes), within the NW massif. Local glacial maximum (Local GM) extent

according to Alonso (1998), Serrano et al. (2012, 2017) and Rodríguez-Rodríguez et al. (2014). Documented cave data is courtesy of the speleological groups reported in Ballesteros et al. (2019a).

Figure 2. Main geomorphological features of the study area (which position is shown in Figure 1) projected on the hillshade digital model. Geomorphology is after Ballesteros et al. (2015, 2017, 2019b), who studied the Pozu Llucia and Torca La Texa shafts.

Figure 3. (A) Aerial photo of the Spanish PNOA 2017 Program projected on a digital elevation model of the Western Massif of Picos de Europa (www.cnig.es; last accessed on May 2019); the star marks the location of Hayéu l'Osu Cave. (B) Topographic restitution of glaciers for the local GM stage, showing the location of the Equilibrium Line Altitude (ELA) and the main ice flow pathways: 1-Ordiales, 2-Hunhumia, 3-Pomperi, 4-El Bricial (4'-Vega de Enol), 5-Ercina, and 6-Belbín.

Figure 4. (A) Geomorphological map of Hayéu l'Osu Cave showing the location of the paleontological sites, the position of dating samples and pictures shown in C, D, E and F. (B) Cave longitudinal profile (P indicates the depth of each shaft in meters, from its top to bottom). (C) Vadose canyon of Stream Gallery showing active channel deposits. (D) Camp Chamber dominated by fluvial terrace deposits. (E) Vadose canyon of Stream Gallery showing fluvial terrace deposits cemented by flowstone and perched above the active channel. (F) Slackwater deposits from the central part of the cavity.

Figure 5. Comparison of the enamel fragment from the Stream Gallery of the Hayéu l'Osu Cave (Figure 4A) with the upper first molars of some extinct and living arvicolines from the Cantabrian Region. Squares in occlusal view (a'–f') are highlighting the buccal salient angle 3 (BSA3). Squares in buccal view (a''–f'') are highlighting the morphology at the base of the BSA3. (A) Enamel fragment found in HAY–9 sample from the study cave. (B) Rooted molars of *Pliomys coronensis* from La Güelga Cave (Figure 1C). (C) Rooted molar of *Clethrionomys glareolus*. Evergrowing molars of: (D) *Arvicola monticola*, (E) *Microtus lavernedii*, and (F) *Microtus lusitanicus*.

Figure 6. Chamois (*Rupicapra pyrenaica*) sites from Hayéu l'Osu Cave: (A) Debris deposit with bone remains (Figure 7A and C-K) in the Llamaeyu Gallery (Figure 4). (B) Location of a scapula (Figure 7B) placed on alluvial deposits of the Stream Gallery (Figure 4).

Figure 7. Chamois (*Rupicapra pyrenaica*) dental and postcranial remains from Hayéu l'Osu Cave. (A) Left M^3 in labial view. (B) Young left scapula in lateral view. (C) Fragment of limb bone diaphysis showing erosion due to transportation by water. (D) Young left radius diaphysis in anterior view showing teeth marks (indicated by white arrows) produced by a small carnivore. (E) Adult right

metacarpal in anterior view. (F) Young left metacarpal in anterior view. (G) Adult proximal phalanx in anterior view. (H) Adult middle phalanx in anterior view. (I) Adult distal phalanx in lateral view. (J) Adult right calcaneus in anterior view. (K) Adult right talus in anterior view. Scale bars are in cm.

Figure 8. Selected sites of Hayéu l'Osu Cave for U-Th and OSL dating: (A) Toppled stalagmite and flowstone originally located on top of slackwater deposits which were subsequently eroded after 263 ka. (B) Perched flowstone precipitated on a first alluvial sequence. (C, D) Second alluvial sequence deposited on flowstone. (E) Second alluvial sequence covered by speleothems. (F) Zoom of sandy layers dated through OSL. (G) Third alluvial pebble sequence with a sandy layer interbedded and dated by means of OSL. Picture locations are shown in Figures 4A and 8.

Figure 9. Cross-section of the surroundings of Covadonga Lakes showing the position of Hayéu l'Osu Cave, Enol and Ercina lakes and Vega de Comeya border polje, which sedimentary infill was previously described and dated in Jiménez-Sánchez and Farias (2002). The position of the cross-section is shown in Figure 2. Bedrock geology is based on Ballesteros et al. (2015). Dates performed in Hayéu l'Osu Cave are detailed in Tables 1, 2 and 3.

Figure 10. Kernel density functions of the OSL, U-Th and radiocarbon ages obtained in the Hayéu l'Osu Cave record, including previous ages from the Vega de Comeya and Enol lacustrine sediments (Moreno et al., 2009; Jiménez-Sánchez et al., 2013). Flowstone precipitation ascribable to the end of MIS 6 fossilized the first detrital sequence identified inside the study cave. The second important episode of cave sediment infill occurred between ca. 98 and 60 ka (phase 1) as glacio-fluvial sediments from a previous glaciation (most likely MIS 5d glaciation) were washed into the cave. The Vega de Comeya sequence indicates that the local Glacial Maximum (local GM) was attained in this area around 45 ± 3 ka (Jiménez-Sánchez et al., 2013), during MIS 3c (phase 2, 48–42 ka). By ~38 ka BP glaciers had already retreated from the Enol Lake depression, allowing proglacial lacustrine sedimentation (Moreno et al., 2010). The retreat of the Ercina glacier front is indirectly recorded in Hayéu l'Osu Cave by the third sedimentary sequence (phase 3, 42–38 ka), suggesting that the Ercina glacier front had also suffered considerable retreat from its previous GM position. The cave entrance and its neighboring areas remained ice-free (phase 4) after ca. 37 ka until, at least, the glacier advance linked to the global LGM of MIS 2 whose extent remains unknown in Picos de Europa (LGM age interval according to Clark et al., 2009).

Figure 11. Paleoenvironmental evolution of the Covadonga Lakes surroundings during MIS 5d–3a illustrated using the cross-section shown in Figure 8 (same legend; see Figure 2 for cross-section location). (A) Phase 1: the study cave recorded detrital sediment input at 98–60 ka, evidencing that the cave setting was an ice-free alpine environment and that eventual glacial fronts were located above 1400 m altitude. (B) Phase 2: glaciers attained their local GM extent at 45 ± 3 ka, causing proglacial lacustrine sedimentation at Vega de Comeya (Jiménez-Sánchez et al., 2013). The Ercina glacier flowed down to 1040 m asl, and La Picota moraine was formed between Ercina and Enol glaciers (Moreno et al., 2010). (C) Phase 3: onset of a general trend of glacial retreat according to Jiménez-Sánchez and Farias (2002). Glaciers receded from the Enol Lake depression at ca. 38 cal ka BP, while Hayéu l'Osu Cave recorded detrital sedimentation since 36 ± 3 ka (HAY-7). (D) Phase 4: occurrence of ice-free temperate environment inhabited by chamois populations.

Figure 12. AMS radiocarbon dates of chamois remains from Llamaeyu and Stream galleries of Hayéu l'Osu Cave, projected over the Greenland $\delta^{18}O$ ice core record (NGRIP, 2004). MIS 3 substages according to Railsback et al. (2015).

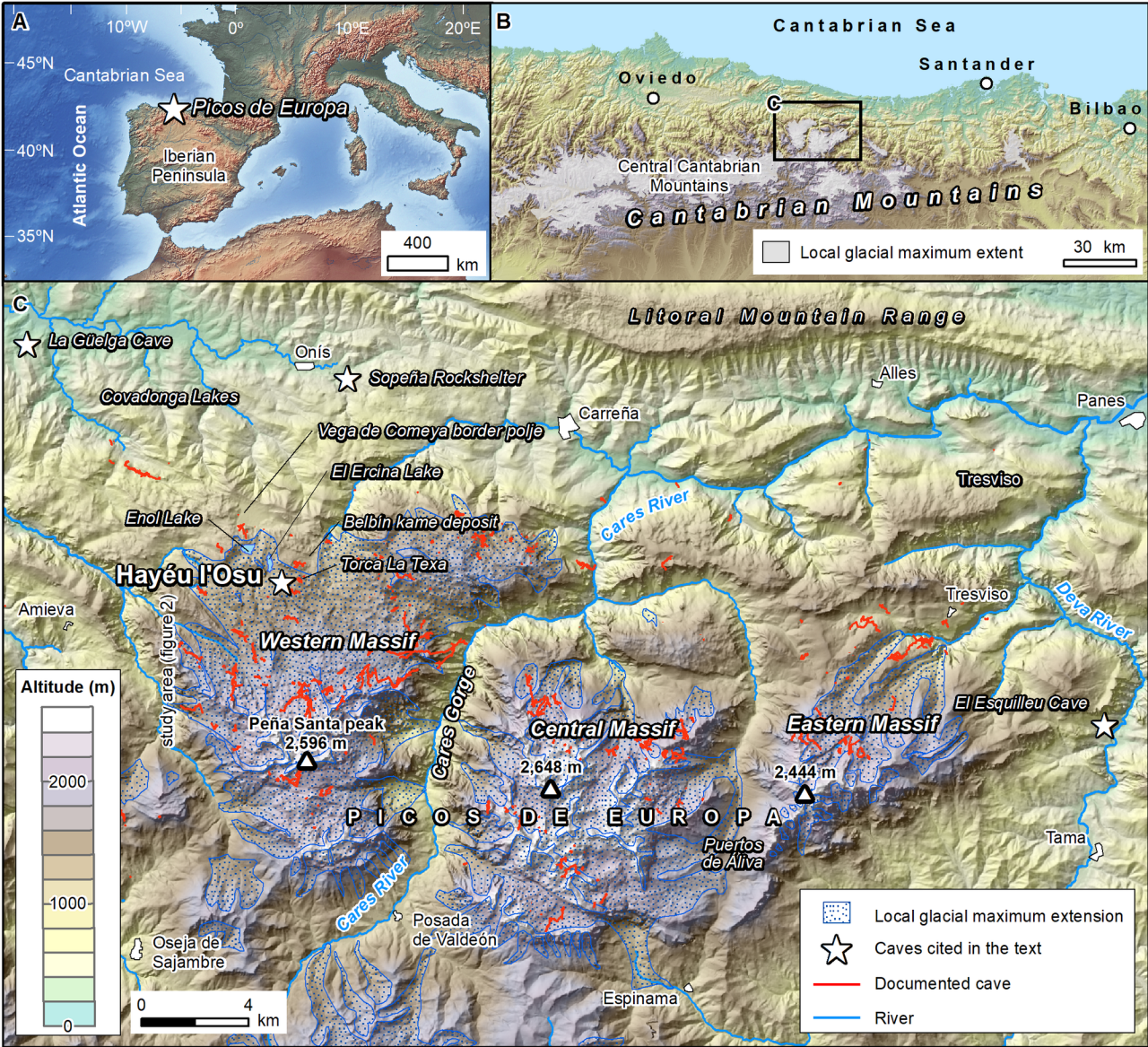
A
10°W
0°
10°E
20°E
45°N
40°N
35°N
Cantabrian Sea
Atlantic Ocean
Picos de Europa
Iberian Peninsula
400
km
B
Cantabrian Sea
Oviedo
Santander
Bilbao
C
Central Cantabrian Mountains
Cantabrian Mountains
Local glacial maximum extent
30 km
C
Litoral Mountain Range
La Güelga Cave
Onís
Sopeña Rockshelter
Covadonga Lakes
Alles
Panes
Carreña
Vega de Comeya border polje
El Ercina Lake
Tresviso
Cares River
Enol Lake
Belbin kame deposit
Torca La Texa
Hayéu l'Osu
Amieva
Tresviso
Deva River
study area (figure 2)
Western Massif
Altitude (m)
2000
1000
0
Peña Santa peak
2,596 m
Cares Gorge
Central Massif
2,648 m
Eastern Massif
El Esquilleu Cave
2,444 m
PICOS DE EUROPA
Puertos de Áliva
Tama
Cares River
Posada de Valdeón
Oseja de Sajambre
Espinama
0
4
km
Local glacial maximum extension
Caves cited in the text
Documented cave
River

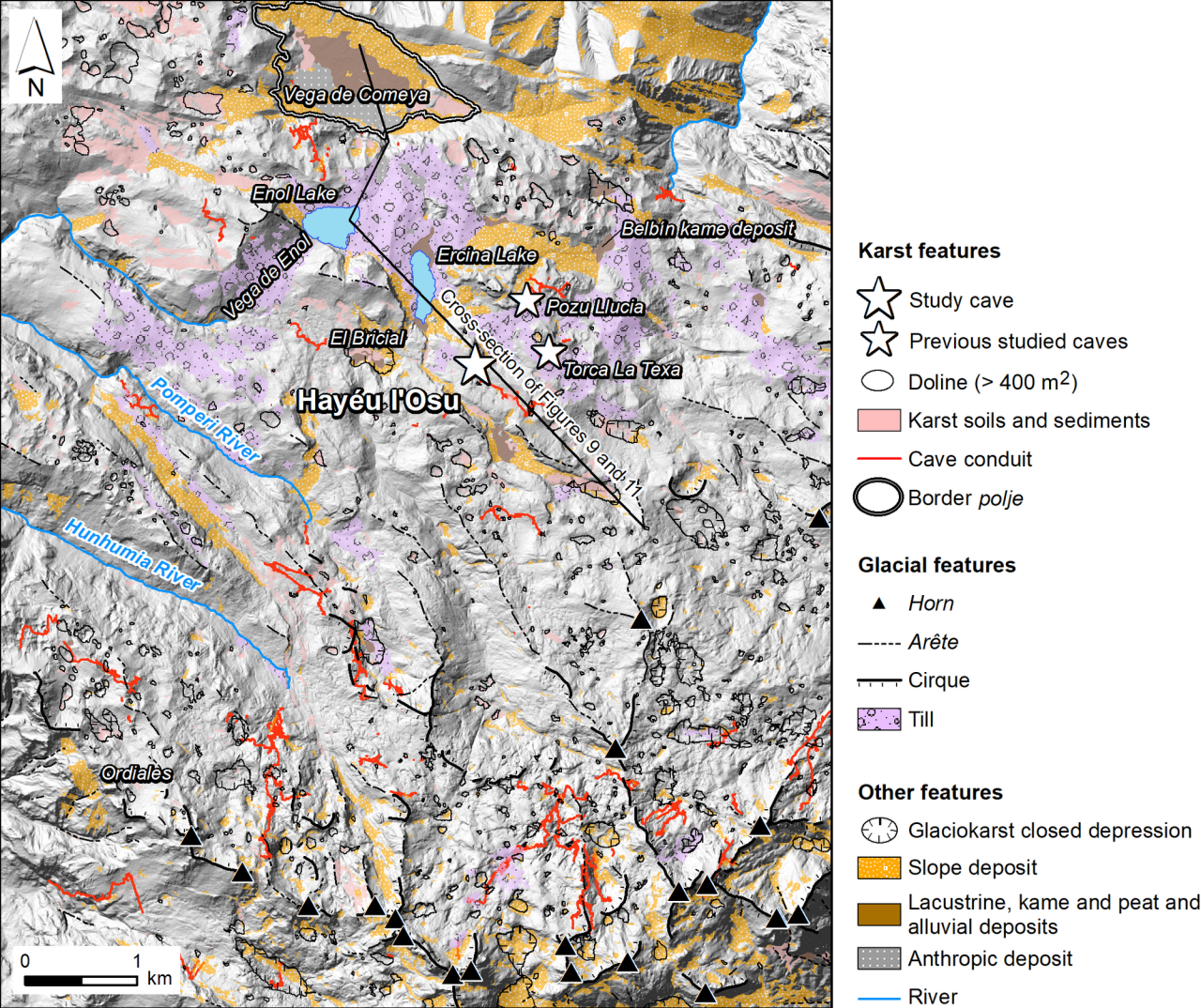
N
Vega de Comeya
Enol Lake
Vega de Enol
Ercina Lake
Belbín kame deposit
Pozu Llucia
Torca La Texa
El Bricial
Cross-section of Figures 9 and 11
Hayéu l'Osu
Pomperi River
Hunhumia River
Ordialès
0
1
km
Karst features
Study cave
Previous studied caves
Doline (> 400 m2)
Karst soils and sediments
Cave conduit
Border polje
Glacial features
Horn
Arête
Cirque
Till
Other features
Glaciokarst closed depression
Slope deposit
Lacustrine, kame and peat and alluvial deposits
Anthropic deposit
River

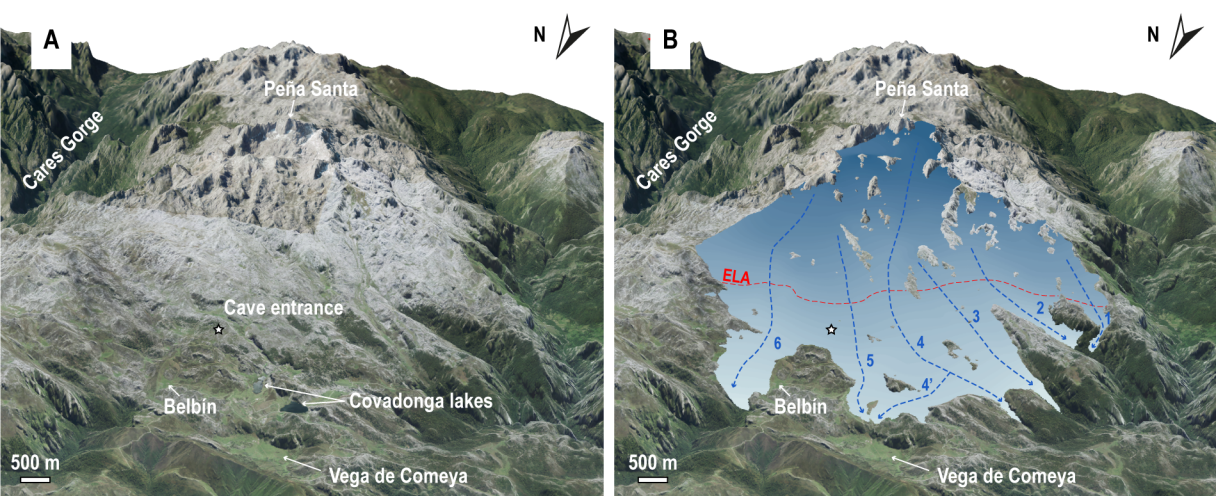
A
N
Peña Santa
Cares Gorge
Cave entrance
Belbín
Covadonga lakes
500 m
Vega de Comeya
B
N
Peña Santa
Cares Gorge
ELA
1
2
3
4
4'
5
6
Belbín
500 m
Vega de Comeya

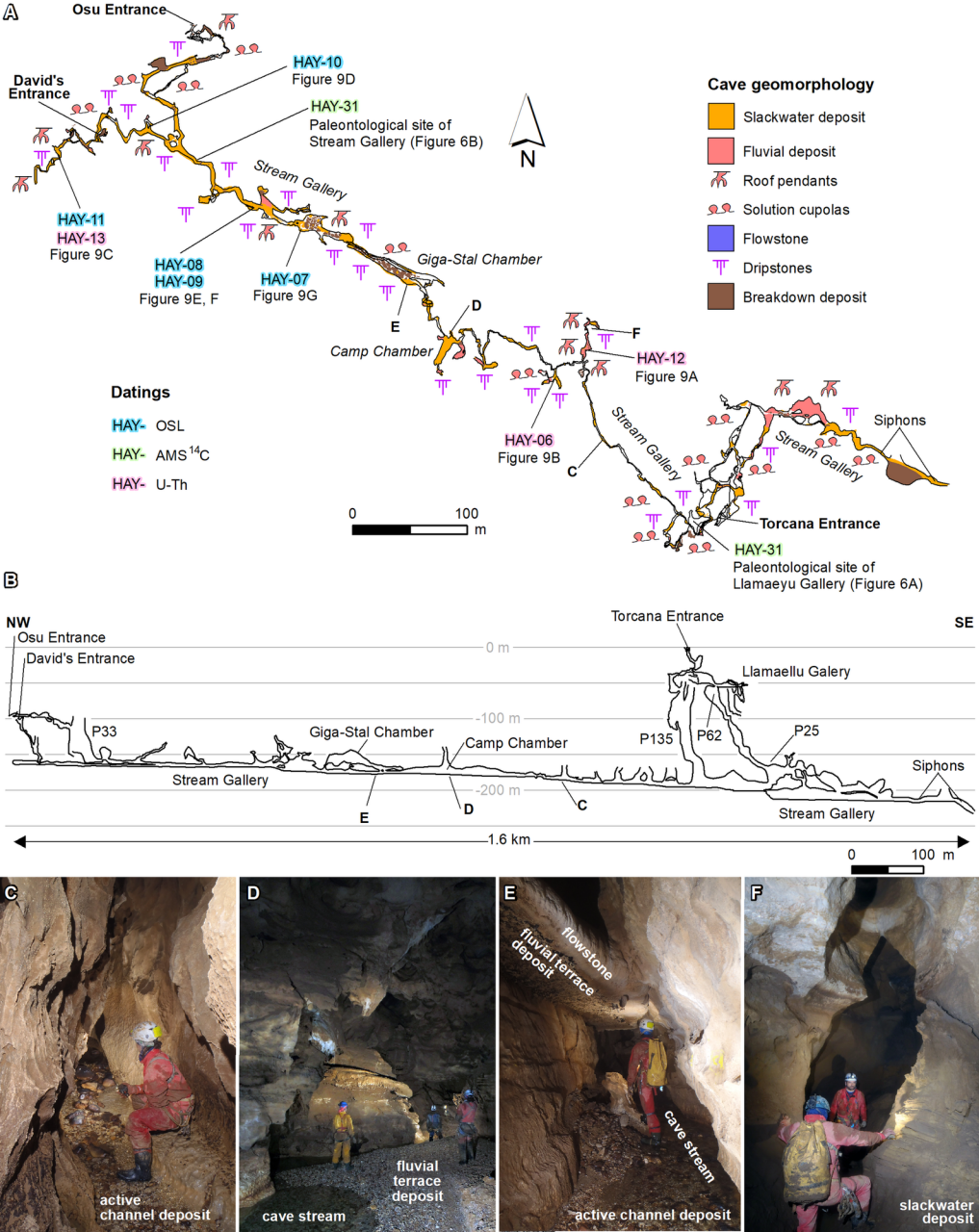
A
Osu Entrance
David's Entrance
HAY-10
Figure 9D
HAY-31
Paleontological site of
Stream Gallery (Figure 6B)
N
Stream Gallery
HAY-11
HAY-13
Figure 9C
HAY-08
HAY-09
Figure 9E, F
HAY-07
Figure 9G
Giga-Stal Chamber
E
D
Camp Chamber
F
HAY-12
Figure 9A
HAY-06
Figure 9B
C
Stream Gallery
Stream Gallery
Siphons
Torcana Entrance
HAY-31
Paleontological site of
Llamaeyu Gallery (Figure 6A)
Cave geomorphology
Slackwater deposit
Fluvial deposit
Roof pendants
Solution cupolas
Flowstone
Dripstones
Breakdown deposit
Datings
HAY- OSL
HAY- AMS 14C
HAY- U-Th
0
100
m
B
NW
SE
Osu Entrance
David's Entrance
Torcana Entrance
0 m
Llamaellu Galery
-100 m
P33
Giga-Stal Chamber
Camp Chamber
P135
P62
P25
Siphons
Stream Gallery
-200 m
E
D
C
Stream Gallery
1.6 km
0
100 m
C
active
channel deposit
D
fluvial
terrace
deposit
cave stream
E
flowstone
fluvial terrace
deposit
cave stream
active channel deposit
F
slackwater
deposit

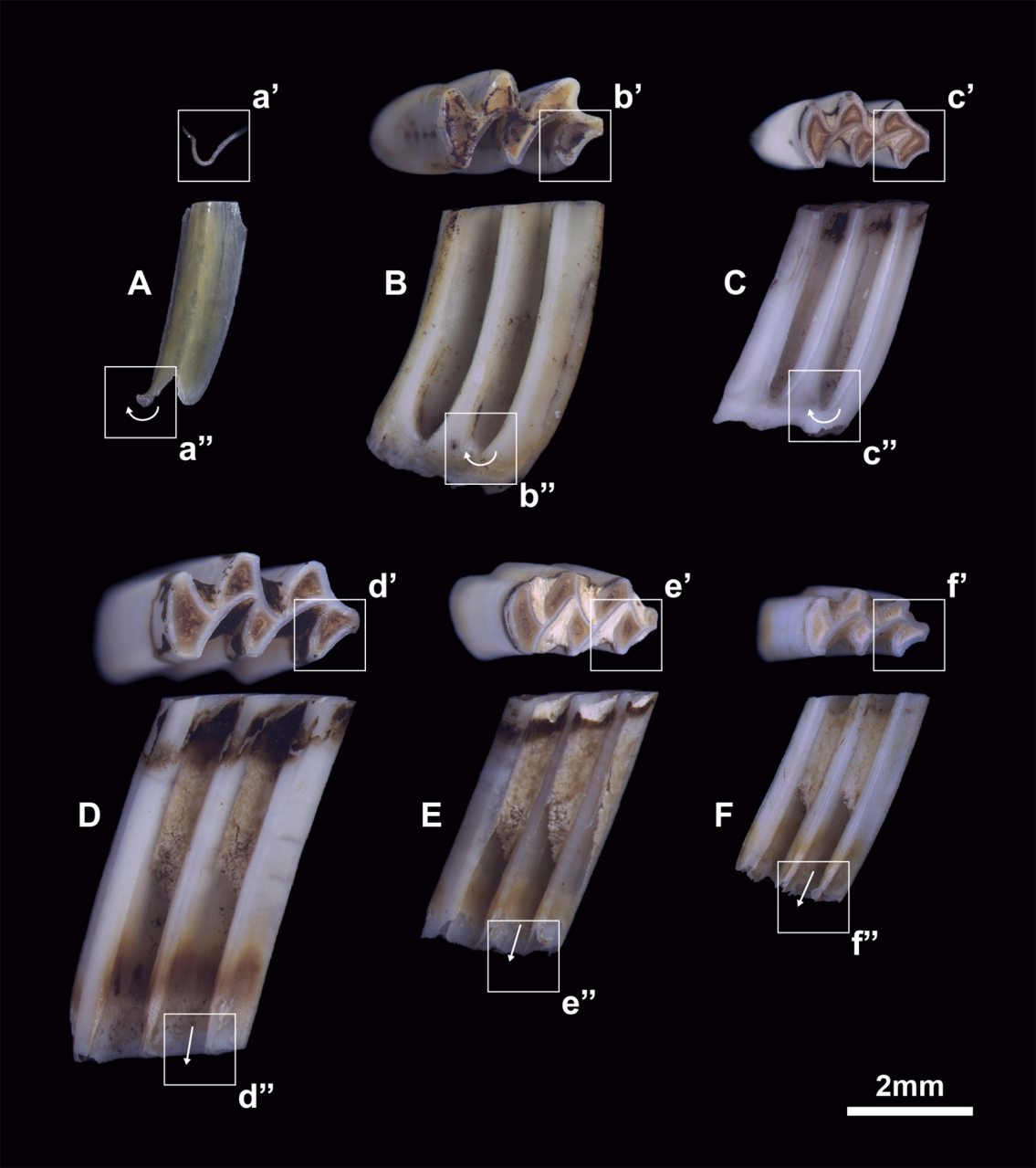
a'
b'
c'
A
B
C
a''
b''
c''
d'
e'
f'
D
E
F
d''
e''
f''
2mm

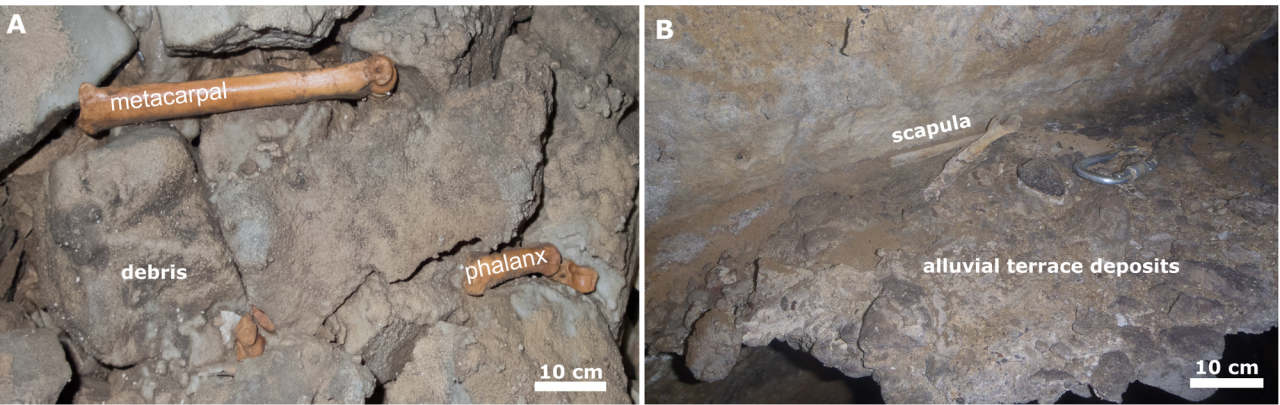
A
metacarpal
debris
phalanx
10 cm
B
scapula
alluvial terrace deposits
10 cm

A
B
C
D
E
F
G
H
I
J
K

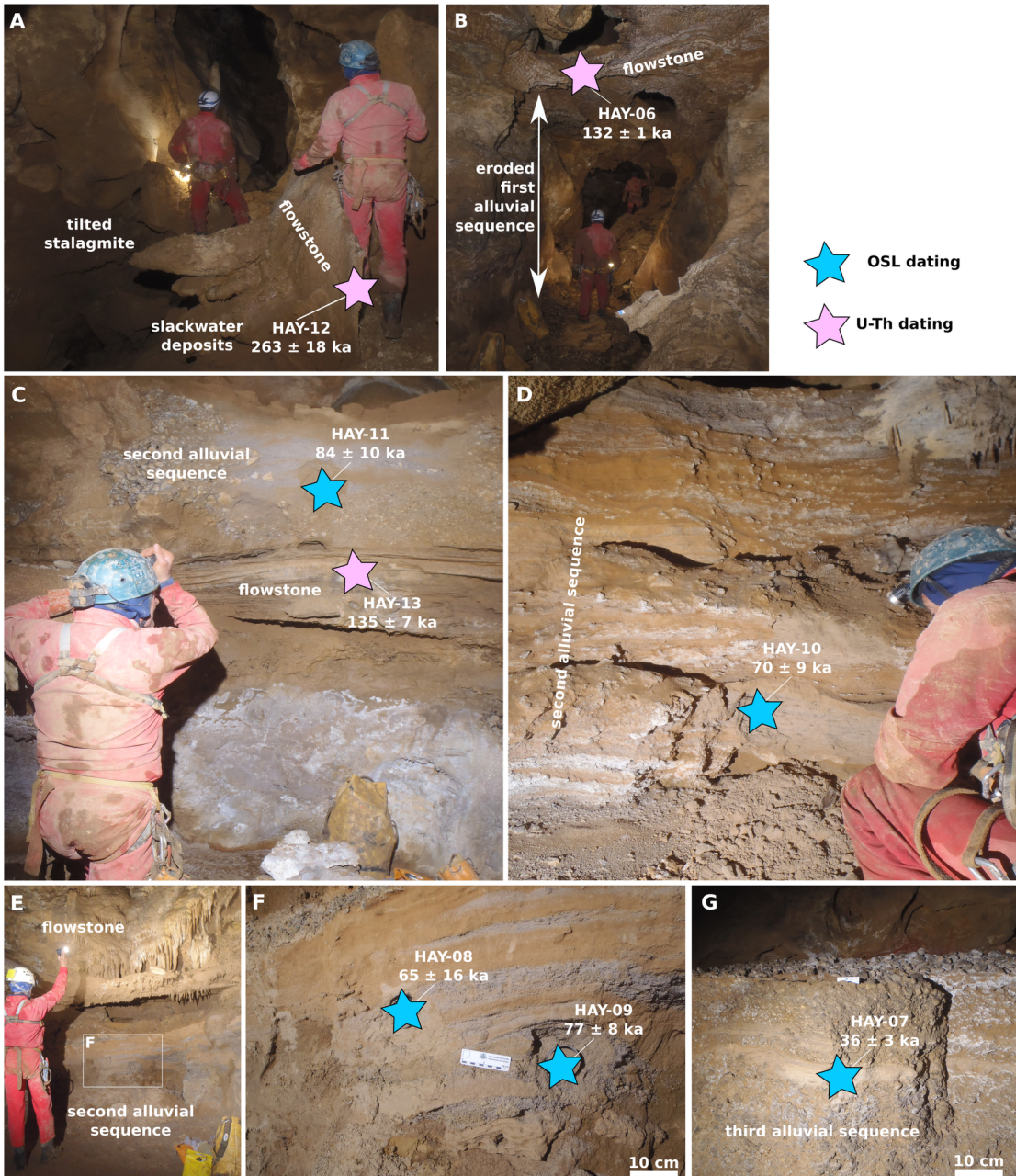
A
tilted stalagmite
flowstone
slackwater deposits
HAY-12
263 ± 18 ka
B
flowstone
HAY-06
132 ± 1 ka
eroded first alluvial sequence
OSL dating
U-Th dating
C
second alluvial sequence
HAY-11
84 ± 10 ka
flowstone
HAY-13
135 ± 7 ka
D
second alluvial sequence
HAY-10
70 ± 9 ka
E
flowstone
F
second alluvial sequence
F
HAY-08
65 ± 16 ka
HAY-09
77 ± 8 ka
10 cm
G
HAY-07
36 ± 3 ka
third alluvial sequence
10 cm

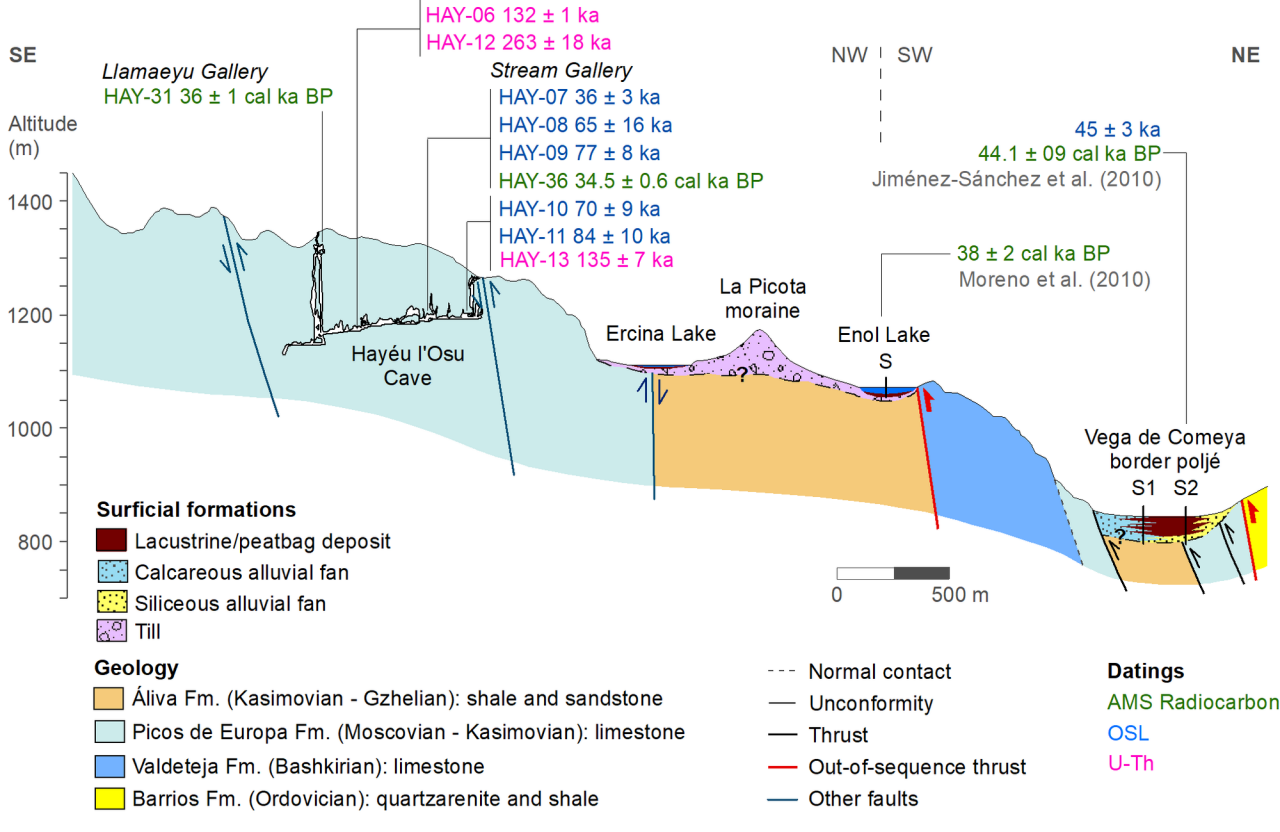
SE
NW
SW
NE
Altitude (m)
1400
1200
1000
800
Llamaeyu Gallery
HAY-31 36 ± 1 cal ka BP
HAY-06 132 ± 1 ka
HAY-12 263 ± 18 ka
Stream Gallery
HAY-07 36 ± 3 ka
HAY-08 65 ± 16 ka
HAY-09 77 ± 8 ka
HAY-36 34.5 ± 0.6 cal ka BP
HAY-10 70 ± 9 ka
HAY-11 84 ± 10 ka
HAY-13 135 ± 7 ka
45 ± 3 ka
44.1 ± 09 cal ka BP
Jiménez-Sánchez et al. (2010)
38 ± 2 cal ka BP
Moreno et al. (2010)
La Picota moraine
Ercina Lake
Enol Lake
S
Hayéu l'Osu Cave
Vega de Comeya border poljé
S1
S2
0
500 m
Surficial formations
Lacustrine/peatbag deposit
Calcareous alluvial fan
Siliceous alluvial fan
Till
Geology
Áliva Fm. (Kasimovian - Gzhelian): shale and sandstone
Picos de Europa Fm. (Moscovian - Kasimovian): limestone
Valdeteja Fm. (Bashkirian): limestone
Barrios Fm. (Ordovician): quartzarenite and shale
Normal contact
Unconformity
Thrust
Out-of-sequence thrust
Other faults
Datings
AMS Radiocarbon
OSL
U-Th

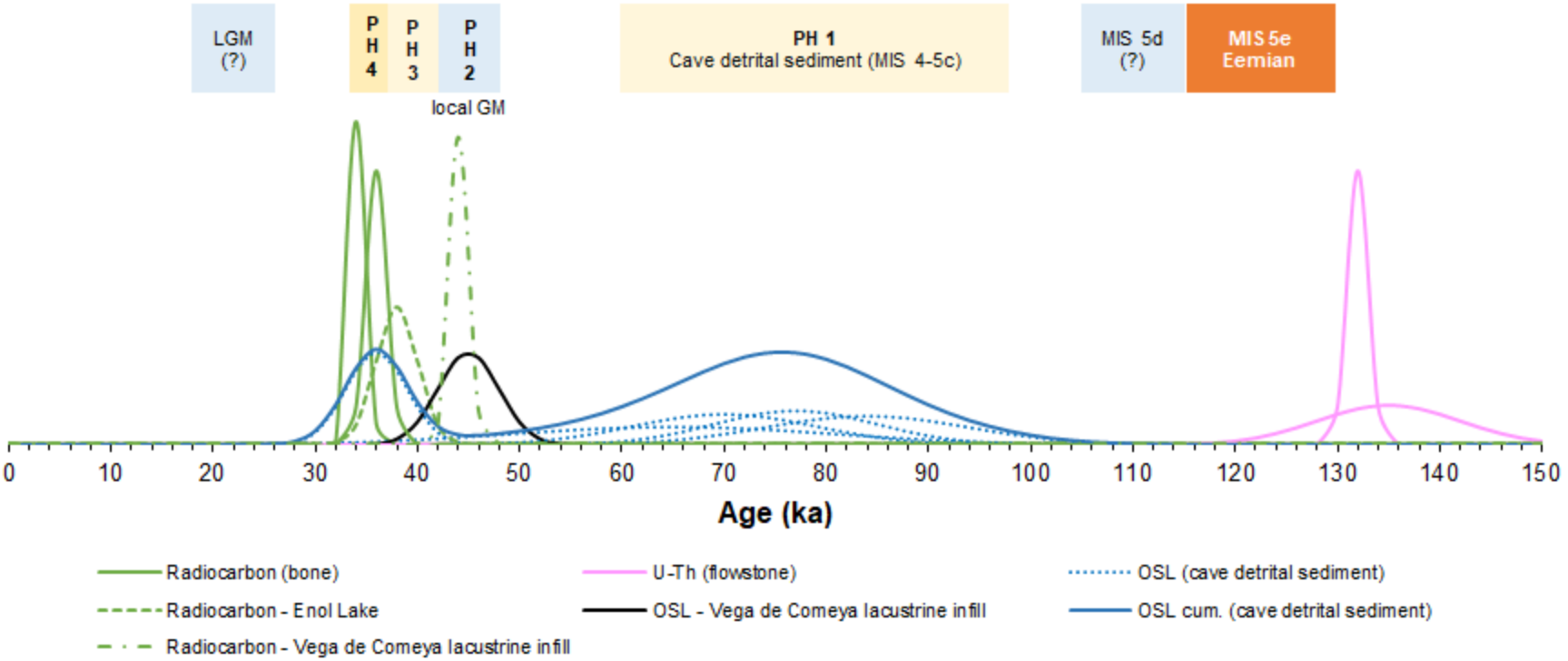
LGM (?)
PH 4
PH 3
PH 2
PH 1
Cave detrital sediment (MIS 4-5c)
MIS 5d (?)
MIS 5e Eemian
local GM
0
10
20
30
40
50
60
70
80
90
100
110
120
130
140
150
Age (ka)
Radiocarbon (bone)
Radiocarbon - Enol Lake
Radiocarbon - Vega de Comeya lacustrine infill
U-Th (flowstone)
OSL - Vega de Comeya lacustrine infill
OSL (cave detrital sediment)
OSL cum. (cave detrital sediment)

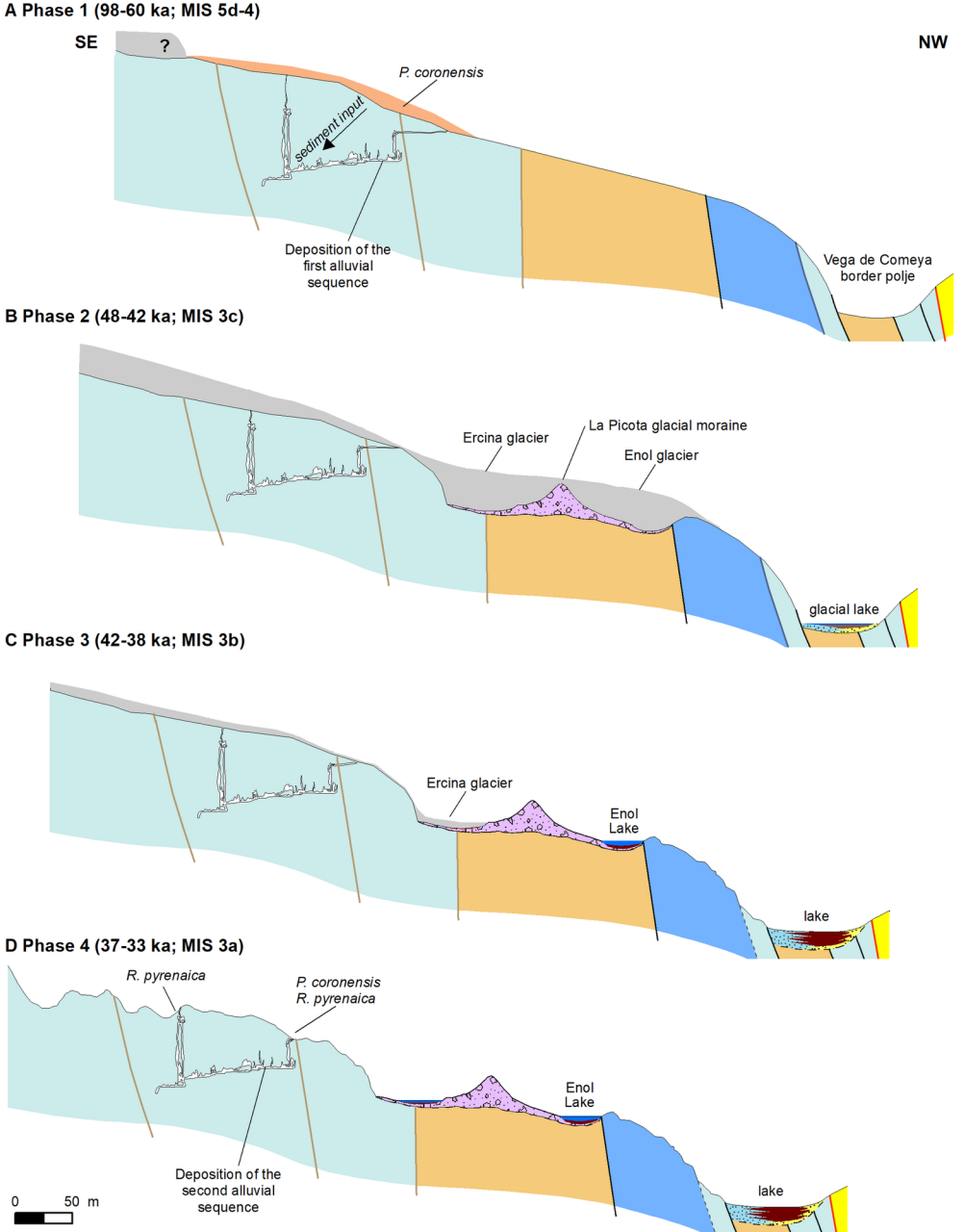
A Phase 1 (98-60 ka; MIS 5d-4)
SE
?
NW
P. coronensis
sediment input
Deposition of the first alluvial sequence
Vega de Comeya border polje
B Phase 2 (48-42 ka; MIS 3c)
Ercina glacier
La Picota glacial moraine
Enol glacier
glacial lake
C Phase 3 (42-38 ka; MIS 3b)
Ercina glacier
Enol Lake
lake
D Phase 4 (37-33 ka; MIS 3a)
R. pyrenaica
P. coronensis
R. pyrenaica
Enol Lake
Deposition of the second alluvial sequence
lake
0
50 m

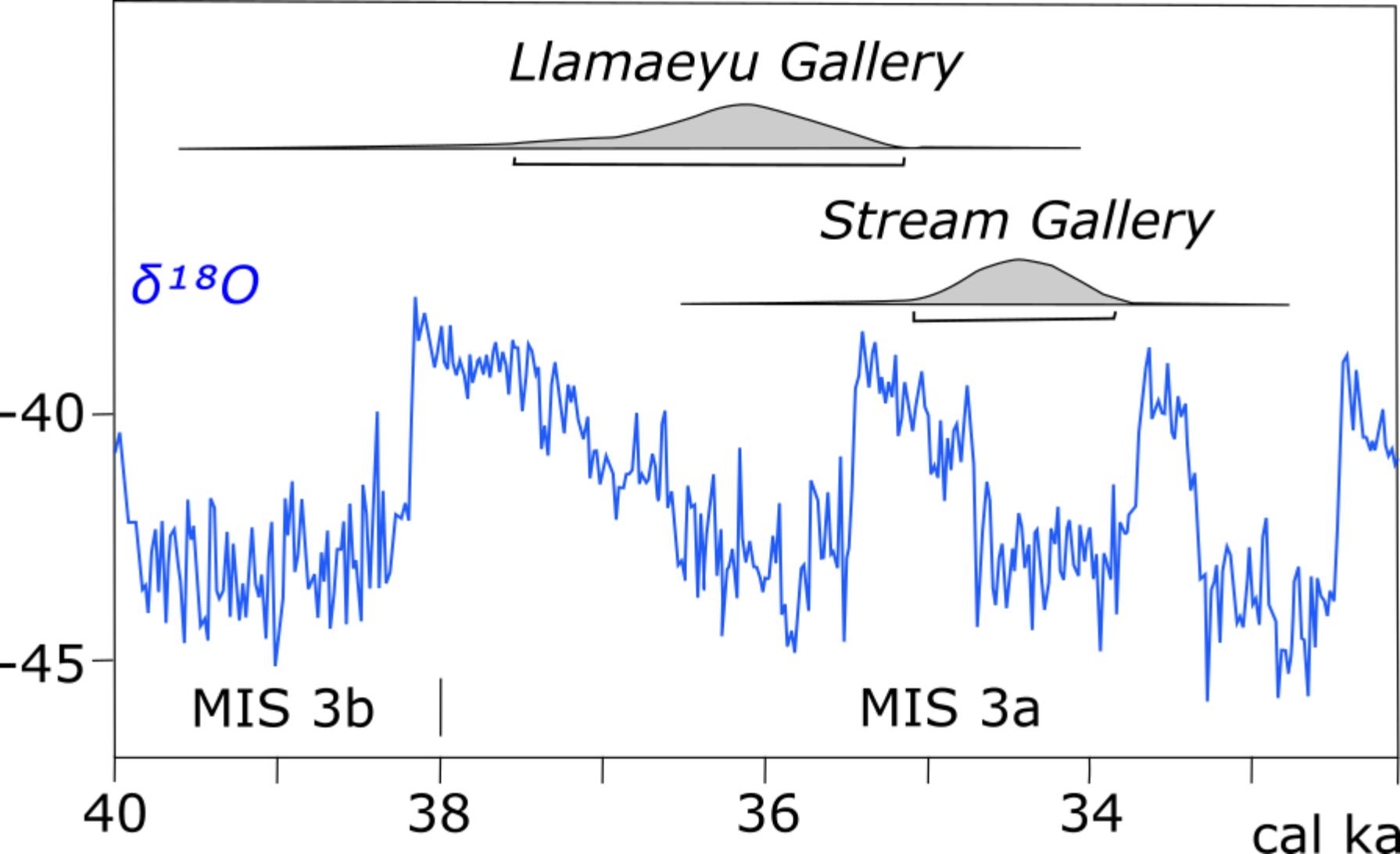
Llamaeyu Gallery
Stream Gallery
δ18O
-40
-45
MIS 3b
MIS 3a
40
38
36
34
cal ka

Table 1. ^{238}U-^{230}Th dating results of Hayéu l'Osu Cave. The error is 2σ. Sample locations are shown in Figures 4A and 8A-C.

Sample	^{238}U (ppb)		^{232}Th (ppt)		^{230}Th / ^{232}Th (atomic $\cdot 10^{-6}$)		$\delta^{234}U$* (measured)		^{230}Th / ^{238}U (activity)		^{230}Th Age (yr) (uncorrected)		$\delta^{234}U_{initial}$** (corrected)		^{230}Th Age (yr BP)*** (corrected)	
HAY-6	65.4	±0.1	8643	±173	293	±6	1994.3	±3.5	2.3433	±0.0072	132630	±732	2892	±10	131570	±1010
HAY-12	28.2	±0.0	48898	±980	16	±0	644.1	±3.4	1.7072	±0.0068	286442	±4903	1353	±68	262977	±17735
HAY-13	95.4	±0.3	66643	±1342	34	±1	793.4	±5.1	1.4240	±0.0063	144811	±1451	1161	±24	134982	±7103

*$\delta^{234}U = ([^{234}U/^{238}U]_{activity} - 1)\cdot 1000$. ** $\delta^{234}U_{initial}$ was calculated based on the ^{230}Th age (T), i.e., $\delta^{234}U_{initial} = \delta^{234}U_{measured}\cdot e^{\lambda 234 x T}$. Corrected ^{230}Th ages assume the initial $^{230}Th/^{232}Th$ atomic ratio of $4.4 \pm 2.2 \cdot 10^{-6}$. Those are the values for a material at secular equilibrium, with the bulk Earth $^{232}Th/^{238}U$ value of 3.8. The errors are arbitrarily assumed to be 50%. *** B.P. stands for "Before Present" where the "Present" is defined as the year 1950 A.D.

Table 2. Optically Stimulated Luminescence (OSL) dates from alluvial sandy sediment samples of Hayéu l'Osu Cave. Figures 4A, 8 and 9C-G show the position of the samples in the study cave.

Sample	**HAY-07**	**HAY-08**	**HAY-09**	**HAY-10**	**HAY-11**
Aliquots (n)	28	4	35	32	35
Equivalent doses (ED) (Gy)	48.4 ± 3.4	35.2 ± 8.4	47.8 ± 3.4	38.3 ± 2.8	44.3 ± 4.3
^{40}K (Bq kg^{-1})	393 ± 13	50 ± 12	79 ± 17	71 ± 14	55 ± 9
^{238}U (Bq kg^{-1})	17 ± 2	18 ± 1	15.6 ± 0.8	18 ± 2	15 ± 2
^{235}U(Bq kg^{-1})	0 ± 0	0 ± 0	0 ± 0	0 ± 0	3.3 ± 2
^{232}Th (Bq kg^{-1})	3.3 ± 0.5	0 ± 0	5.5 ± 0.8	0 ± 0	0 ± 0
Beta radiation dose	0.89 ± 0.04	0.31 ± 0.04	0.35 ± 0.04	0.31 ± 0.04	0.29 ± 0.04
Gamma radiation dose	0.39 ± 0.02	0.17 ± 0.01	0.21 ± 0.02	0.16 ± 0.02	0.17 ± 0.01
Cosmic radiation dose	0.06 ± 0.003	0.06 ± 0.003	0.06 ± 0.003	0.07 ± 0.003	0.07 ± 0.003
Dose rate (DR) (Gy ka^{-1})	1.34 ± 0.4	0.54 ± 0.04	0.62 ± 0.05	0.55 ± 0.06	0.53 ± 0.04
Overdispersion (%)	26.3 ± 5.8	38.9 ± 20.0	24.3 ± 5.5	26.1 ± 6.4	38.8 ± 8.7
Age (ka)	36 ± 3	65 ± 16	77 ± 8	70 ± 9	84 ± 10

Table 3. Calibrated AMS radiocarbon dates of chamois (*R. pyrenaica*) assemblage of Hayéu l'Osu Cave. The position and remains of the paleontological sites is shown in Figures 4A, 7 and 8.

Sample	**Paleontological sites**	**Conventional age** (years BP)	**Calendar age** (2σ) (years BP)
HAY-31	Stream Gallery	32220 ± 440	37534–35139
HAY-36	Llamayeu Gallery	30440 ± 360	35076–33836

Table 4. Synthesis of the paleoenvironmental evolution of Picos de Europe during MIS 5c to 3. See Section 5 and Figures 10 and 11 for details.

Phase	Age (ka)	MIS	Main event	Paleoenvironment at a reference altitude of 1400 m	Evidence from the study cave	Evidence from previous works
1	98-60	5c–4	Glacier retreat	Area with rocky outcrops and fluvioglacial sediments. Probably glaciers in upper areas. Relative cold conditions	Deposition of the second alluvial sequence in the cave Occurrence of *Pliomys coronensis*	
2	48-42	3c	Local glacial maximum advance	Area covered by glaciers		Glacio-lacustrine sedimentation in Vega de Comeya border polje at 850 m asl (Jiménez-Sánchez et al., 2013)
3	42-38	3b	Onset of glacier retreat	Probably, area covered by glaciers		Glacio-lacustrine sedimentation at Enol Lake at 1075 m asl (Moreno et al., 2009)
4	37-33	3a	Glacier retreat	Area with rocky outcrops and fluvioglacial sediments; relative cold conditions	Deposition of the third alluvial sequence in the cave Occurrence of *Rupicapra pyrenaica*	